nature protocols

https://doi.org/10.1038/s41596-025-01306-w

Protocol

Check for updates

Conjugation of hydrophobic drugs to motile pRNA 4WJ nanoparticles for spontaneous tumor targeting and undetectable toxicity

Daniel W. Binzel[1,2,3] ✉, **Kai Jin**[1,2,3], **Tesla Yudhistira**[1,2,3] & **Peixuan Guo**[1,2,3,4] ✉

Abstract

Chemotherapeutics are widely used in cancer treatments, but their toxicity, bioavailability and solubility present challenges. RNA nanotechnology has emerged as a promising modality for targeted delivery of chemotherapeutics. Structurally, RNA is thermostable, while conformationally it is dynamic and flexible. RNA's unique deformability and motility lead to rapid spontaneous tumor accumulation and glomerular excretion, thus fast body clearance, while its anionic charge and favorable small size prevent accumulation in vital organs, resulting in undetectable toxicity. We developed branched 4-way junction (4WJ) nanoparticles that were stable with a melting temperature >80 °C, even when conjugated with 24 drugs per 4WJ. Each 4WJ RNA component strand can conjugate six molecules of hydrophobic chemotherapeutic drugs, such as camptothecin, paclitaxel and SN-38. Thus, each 4WJ carries a total of 24 drug molecules spaced to prevent aggregation. RNA conjugation improved paclitaxel water solubility 32,000-fold. This protocol describes the construction of 4WJ RNA drug complexes for cancer therapy. Specific procedures include the modification of chemical drugs, conjugation of multiple prodrug molecules to each synthesized RNA component strand, assembly of RNA nanoparticles and their purification and characterization. Prodrugs are conjugated to RNA nanoparticles via efficient click chemistry, creating an ester linker that is cleaved by esterases in tumor tissues or cells, allowing the prodrugs to return back to their original structures and chemistry upon delivery and release, minimizing toxicity. Inclusion of tumor targeting ligands demonstrated specific delivery of high payload chemotherapeutics to tumors, controlled release of chemical drugs and strong tumor inhibition.

Key points

- RNA strands containing modified nucleotides are produced by using solid-phase synthesis for conjugation with multiple chemotherapeutic prodrugs, including camptothecin, paclitaxel and SN38, by copper-chelated click chemistry, where copper is easily removed during purification due to its much smaller size compared to RNA before assembling the 4WJ RNA nanoparticles, which can be loaded with up to 24 drug molecules per nanoparticle.
- The RNA nanoparticles can be designed to contain a tumor-targeting ligand, resulting in specific uptake by the target cell type, while the drug payload is released via cleavage by esterases in the tumor microenvironment to ensure site-specific delivery.

Key references

Guo, S. et al. *Nat. Commun.* **11**, 972–982 (2020): https://doi.org/10.1038/s41467-020-14780-5

Piao, X. et al. *Adv. Sci.* **6**, 1900951 (2019): https://doi.org/10.1002/advs.201900951

Li, X. et al. *Biomaterials* **305**, 122432 (2023): https://doi.org/10.1016/j.biomaterials.2023.122432

[1]Center for RNA Nanobiotechnology and Nanomedicine, The Ohio State University, Columbus, OH, USA. [2]Division of Pharmaceutics and Pharmacology, College of Pharmacy, The Ohio State University, Columbus, OH, USA. [3]Comprehensive Cancer Center, The Ohio State University, Columbus, OH, USA. [4]College of Medicine, The Ohio State University, Columbus, OH, USA. ✉e-mail: binzel.2@osu.edu; guo.1091@osu.edu

Introduction

Chemotherapeutics are a popular and effective method in cancer therapy, because small molecules can enter and inhibit rapidly dividing cells with fast metabolic processes. However, many chemotherapeutics face the challenges of unfavorable bioavailability, poor cellular transport and indiscriminate targeting of cells. As a result, patients treated with chemotherapeutics suffer from high levels of toxicity to healthy organs and poorly tolerate delivered doses. Chemotherapeutics have undergone reformulations into less-toxic prodrugs or nanoparticle conjugates by enhancing specific delivery and reducing toxicity[1–4]. However, the development of chemoresistance and recurrence in late stage in cancer has become a challenging problem[3,5,6]. There is a great need for on-tumor delivery of chemotherapeutics that can overcome the above-mentioned limitations. Antibody–drug conjugates (ADCs) have recently come to the market and specifically bind therapeutic targets on tumors, while also delivering chemotherapeutic cargoes or conjugates. This on-target delivery has generated great interest, with >240 clinical trials in 2024 (refs. 7–9). ADCs have greatly advanced drug delivery, but because of the amphiphilic nature of proteins and their relatively larger size, they can generate side effects and toxicities from immune responses, they suffer from early release of chemotherapeutics and are prone to aggregation[10].

The discovery of a small noncoding packaging RNA (pRNA) in the genome of the bacteriophage Phi29 (ref. 11) and the special hand-in-hand interactions[12] that form hexameric rings led to the emergence of RNA nanotechnology[13]. It was previously predicted that RNA therapeutics would be the third milestone in pharmaceutical drug development[14]. The clinical application of RNA has rapidly gained interest after the successful development of mRNA vaccines during the severe acute respiratory syndrome coronavirus 2 pandemic[15–17] along with the US Food and Drug Administration approval of Onpattro (patisiran) as the first RNA therapeutic, followed by approval of subsequent therapeutics[18]. Within RNA therapeutics, RNA nanotechnology has developed into a promising field that has demonstrated both spontaneous and active targeting to cancer tumors in mouse models[19–21]. RNA nanoparticles self-assemble from several short RNA oligonucleotides (oligos) into stable branched motifs[13], allowing for functionalization through conjugation of additional groups such as RNA aptamer or chemical targeting ligands[22–27], interfering RNA (iRNA) (including small interfering RNA (siRNA), microRNA (miRNA) and anti-miRNA)[28–36], fluorescent or radioactive markers[27,37–39], ribozymes[22,40] and chemotherapeutics[41–45]. RNA nanoparticles, including their core motif and functional groups, are primarily composed of RNA, and their design has been discussed at length in several high-profile reviews[13,19,46–48]. RNA nanoparticles are motile and deformative, allowing for their rapid and spontaneous accumulation in tumors, because the RNA nanoparticle can deform and squeeze through leaky tumor vasculature[19–21]. In addition, these properties allow for rapid renal clearance of non-tumor accumulated nanoparticles, resulting in safe biodistribution profiles[20,49]. The addition of RNA aptamers that target tumor-associated receptors allows for active tumor targeting of tumors and endocytosis into tumor cells for efficient cargo delivery[29–33,50]. Finally, the immunogenicity of RNA nanoparticles is tunable by modulating nanoparticle sequence, size, shape and stoichiometry, allowing for the generation of safe RNA nanoparticles with no immune response[51–54].

Development of the protocol

The feasibility of RNA nanotechnology was first proven through the controlled assembly of nanorings composed of pRNA from the Phi29 DNA packaging motor[12]. The formation of RNA rings composed of multiple RNA subunits led to the idea of developing RNA nanoparticles for therapeutic applications[55]. The Phi29 pRNA hexameric ring was conceptualized to carry a functional module off each pRNA and proven as a functional nanoparticle through the combination of one pRNA harboring a cell targeting ligand and a second pRNA extended to include an siRNA[28,55,56]. Through the years, new RNA nanoscaffolds were developed to greatly improve the branched structuring for including more functional modules and drastically improve the enzymatic and thermodynamic stabilities[40,47,51,57–69]. Thus, RNA nanoparticles have demonstrated the ability to serve as a therapeutic platform delivering nucleic acid–based therapies including siRNA, miRNA and anti-miRNA. We have previously published a protocol on the development of RNA nanoparticles for the delivery of therapeutic RNAs[70,71]. The resulting RNA nanoparticles were able to accumulate in tumor microenvironments and successfully delivered functional modules to silence specific genes, resulting in tumor growth inhibition[29,30,32,33,57,72–77].

Recently, RNA nanoparticles were designed for the purpose of conjugating and solubilizing hydrophobic chemical drugs, including delivering paclitaxel (PTX), camptothecin (CPT) and SN38 (refs. 41–44). Since unusual thermostability of the Phi29 pRNA three-way junction (3WJ) with a high melting temperature (T_m) was reported[57], branched RNA nanoparticles have been extensively investigated for their potential for iRNA and chemical drug delivery[41]. We developed an RNA 4WJ, derived from the Phi29 pRNA-3WJ. The resulting 4WJ has higher thermodynamic stability and can thus carry more chemical drugs. This 4WJ was found to form quickly at a high annealing temperature (T_a) of 80.9 °C compared to 58.4 °C of the smaller pRNA-3WJ and resulted in increased drug payload on 24 molecules compared to only 10 molecules for the pRNA-3WJ[41]. The 4WJ nanoparticle is a rather small nanoparticle, slightly smaller than 10 nm and simplistic in that it is composed of four short (approximately 40 nt) oligo strands that rely on base pairing to form its highly stable structure. Because of the unique capabilities of the 4WJ nanoparticle, PTX conjugation resulted in enhancing the drug solubility 32,000-fold[41]. The resulting 4WJ RNA drug complex spontaneously accumulated in tumors within 30 min after intravenous administration, even without ligands[20,39]. For non-tumor-accumulated nanoparticles, fast renal excretion and rapid body clearance results in little organ accumulation, undetectable toxicity and no immunogenicity. Safety parameters such as organ histology, blood biochemistry and pathological analysis have been reported[44]. The highly efficient tumor growth inhibition, undetectable toxicity and favorable chemistry, manufacturing and controls production of these RNA nanoparticles generates a candidate with high potential for translation in cancer therapy. As such, RNA nanoparticles have a bright future in the pharmaceutical field and are part of the third milestone in pharmaceutical drug development[14].

The transition of producing RNA nanoparticles via solid-phase chemical synthesis from in vitro transcription allowed for the inclusion of chemically modified nucleotides within RNA nanoparticles. The available wide array of chemically modified phosphoramidites allow for production of 4WJ with diverse nucleotide structures[41–43,64] as compared to those that were produced by biological RNA polymerases[78–81]. Click chemistry, first developed by K. B. Sharpless[82,83], provides simple and efficient chemical reactions that are easily adaptable for linking biological molecules through the use of organic chemical groups. Solid-phase synthesis approaches using modified phosphoramidites, such as including alkyne modifications, make it possible to apply highly efficient click chemistry to RNA nanotechnology. For example, the 2′-propargyl modifications can be achieved for multiple nucleotides in the RNA strand[41,43]. Click chemistry simplified synthetic chemistry techniques needed for the conjugation of chemotherapeutic prodrugs to RNA oligos while maintaining a high yield and reaction selectivity. The azide alkyne Huisgen cycloaddition reaction[82,84], used in this protocol, provided a feasible drug conjugation to RNA oligos in a single step.

This protocol presents the development of thermodynamically and enzymatically stable 4WJ RNA nanoparticles capable of targeting tumors and delivering conjugated chemotherapeutics safely and effectively[41,43]. Developed 4WJs are synthesized with 24 molecules of various chemotherapeutic prodrugs, including PTX, CPT and SN38 (refs. 41–43). The high tumor accumulation of the nanoparticles results in specific chemotherapeutic release of prodrugs into authentic drugs as the prodrugs are cleaved into their original chemical structure by tumor-associated esterases in the tumor microenvironment, diminishing the toxicity and side effects of the delivered chemotherapeutics[44].

Overview of the Procedure

This protocol covers the steps for producing thermostable 4WJ RNA nanoparticles with hydrophobic chemical drugs and characterizing the nanoparticles' biophysical characteristics and anti-cancer efficacy. The protocol covers the synthesis of RNA oligos, production of

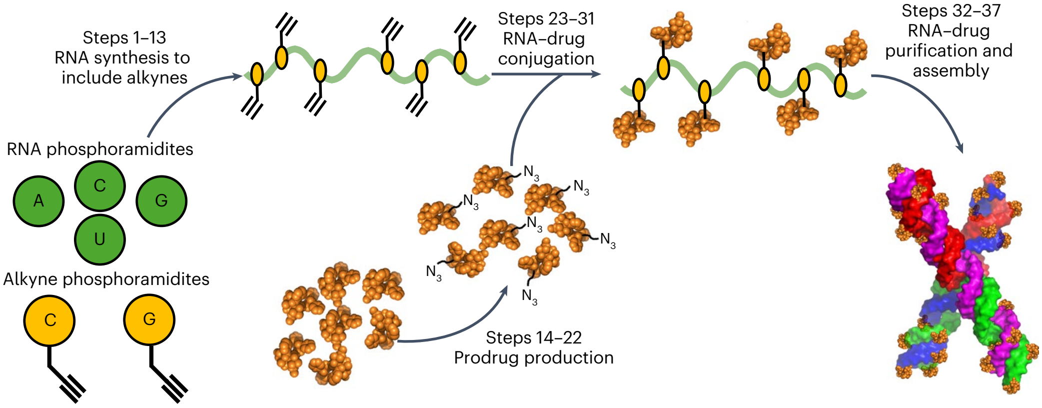

Fig. 1 | Overview schematic of the procedure to produce a branched RNA nanoparticle conjugated with small-molecule chemical drugs. Adapted with permission from ref. 41, CC BY 4.0 (https://creativecommons.org/licenses/by/4.0/).

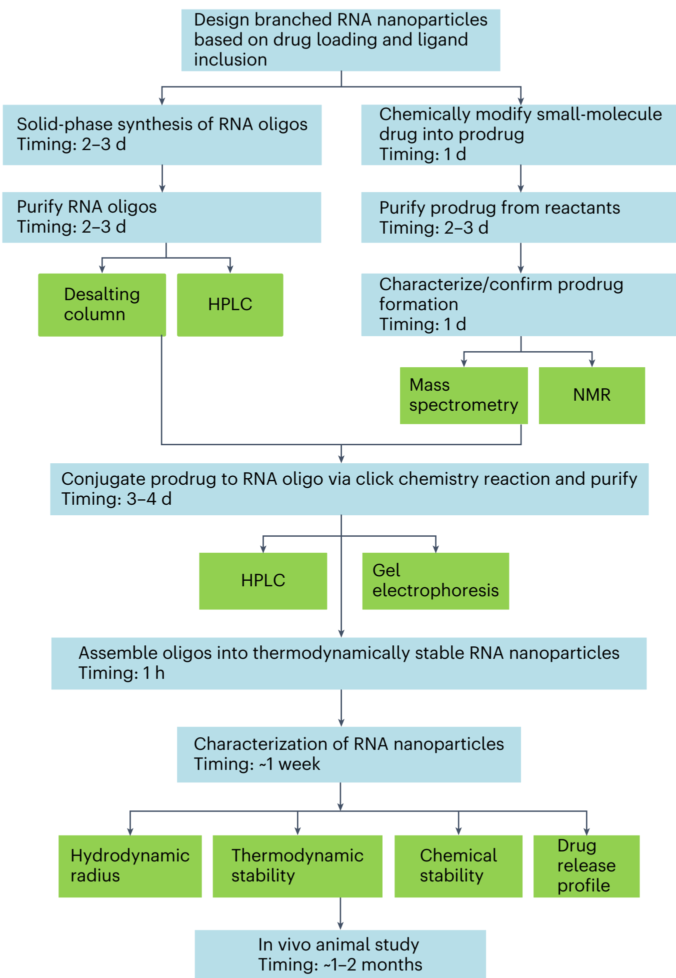

Fig. 2 | Workflow of the procedure for generating chemical drug-conjugated RNA nanoparticles. Outlined steps, including estimated time to complete, for the synthesis and testing of drug-conjugated RNA nanoparticles.

chemotherapeutic prodrugs, conjugation of prodrugs to RNA and finally the assembly and purification of RNA 4WJ nanoparticles (Fig. 1). A flow chart of the procedure highlighting the estimated timing of each stage is provided in Fig. 2.

The production of RNA nanoparticles conjugated with chemical drugs begins with the design of the RNA nanoparticle itself. RNA nanoparticles of various sizes, shapes and

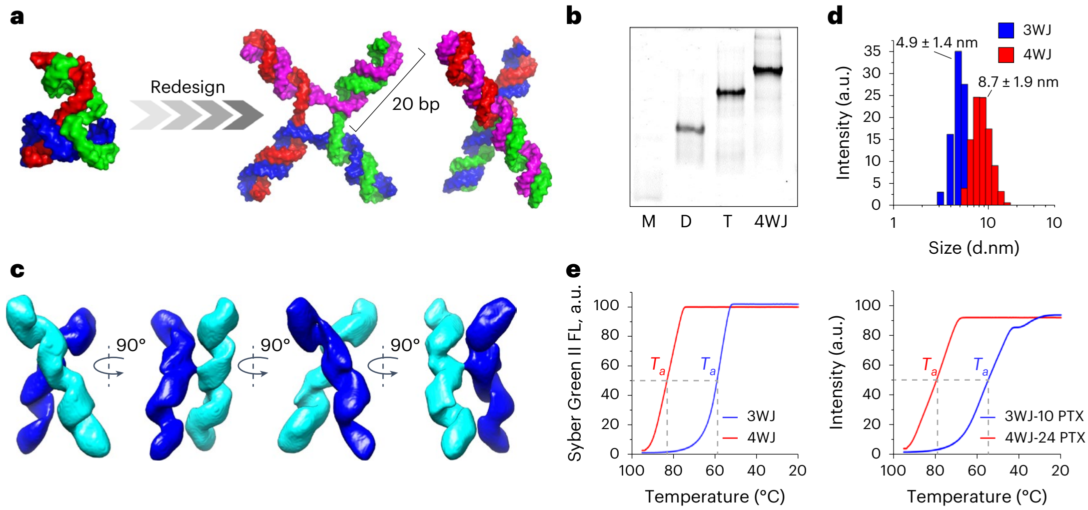

Fig. 3 | Overview of an ultra-stable 4WJ RNA nanoparticle for chemical drug conjugation. a, Predicted structure of the 4WJ RNA nanoparticle (right) derived from the Phi29 pRNA-3WJ (left). **b**, Twelve per cent (wt/vol) native PAGE in TBE showing assembly of the 4WJ RNA nanoparticle from four short RNA oligos showing high assembly yield. **c**, Cryo-EM reconstruction of the 4WJ RNA nanoparticle matching predicted structures. **d**, Dynamic light scattering of the 4WJ RNA nanoparticle (red) compared to the 3WJ (blue), both showing homogeneous products. **e**, Thermostability of the 3WJ and 4WJ RNA nanoparticles without (left) and with (right) PTX conjugation, showing strong increased T_a of the 4WJ by SYBR Green II fluorescence (FL) measured by using a thermocycler. a.u., arbitrary units; D, dimer; M, monomer; T, trimer. Panels **a**–**c** reproduced and panels **d** and **e** adapted from ref. 41, CC BY 4.0 (https://creativecommons.org/licenses/by/4.0/).

sequences have been constructed to include branched motifs (3WJ[57,85–87], 4WJ[41,43,88,89], six-way junction (6WJ)[34], etc.), 2D planar geometric shapes (triangle, square and pentagon)[51,61,90–93], 3D shapes (tetrahedron, prisms and dodecahedron)[60,94–96] and micellular structures[64,97]. These various nanoparticles are highlighted in our previous *Nature Protocols* and *Chemical Reviews* publications[19,70]. For conjugation of chemotherapeutics, it is important to ensure that the RNA nanoparticle remains stable after drug conjugation while preventing drug aggregation[41]. The conjugation of chemotherapeutics can affect the base pairing of the nucleotides, resulting in low thermostability of the nanoparticle. As an example, the conjugation of PTX to the Phi29 pRNA-3WJ resulted in greatly reducing the thermostability of the normally stable 3WJ[41]. For this requirement, RNA nanoparticle design must be taken into consideration to ensure high thermostability. Furthermore, high G:C content of RNA has been commonly believed to be more thermodynamically stable, and one would consider mutating an RNA junction's sequence to improve thermostability. However, such mutations were found to be detrimental to the junction's structuring by Li et al.[43]. In addition, the RNA nanoparticle must be designed to have ≥5 nt between drug conjugation sites to ensure that drugs do not aggregate and do not alter the 4WJ folding, while the strand sequence must be long enough to allow for high drug loading[41,43]. The RNA 4WJ used in this protocol is derived from Phi29 pRNA-3WJ[41,57] (Fig. 3a). The 4WJ carries 24 drug conjugation sites while maintaining proper drug spacing. The high thermostability of the 4WJ is critical for maintaining stability upon drug conjugation. An additional nanoparticle design component is the inclusion of fluorophore(s) for tracking RNA targeting and distribution[37] or cancer targeting ligands, such as folate[55,57], epidermal growth factor receptor (EGFR) RNA aptamer[98] and epithelial cell adhesion molecule (EpCAM) RNA aptamer[99].

Next, RNA oligos that compose the 4WJ RNA nanoparticle must be produced. Synthesis of RNA can generally occur via in vitro transcription using a T7 polymerase or via solid-phase chemical synthesis. Each method has its advantages; however, chemical synthesis is required in this protocol because it allows for the use of chemically modified nucleotide phosphoramidites to incorporate chemical moieties used for drug conjugation[41–44] (Fig. 1). Each of the four oligo strands is synthesized to include six 2′-propargyl modified nucleotides to provide alkyne groups used later in click chemistry conjugation of chemotherapeutic prodrugs. Synthesized RNA strands are purified by standard desalting procedures, reverse-phase high-performance

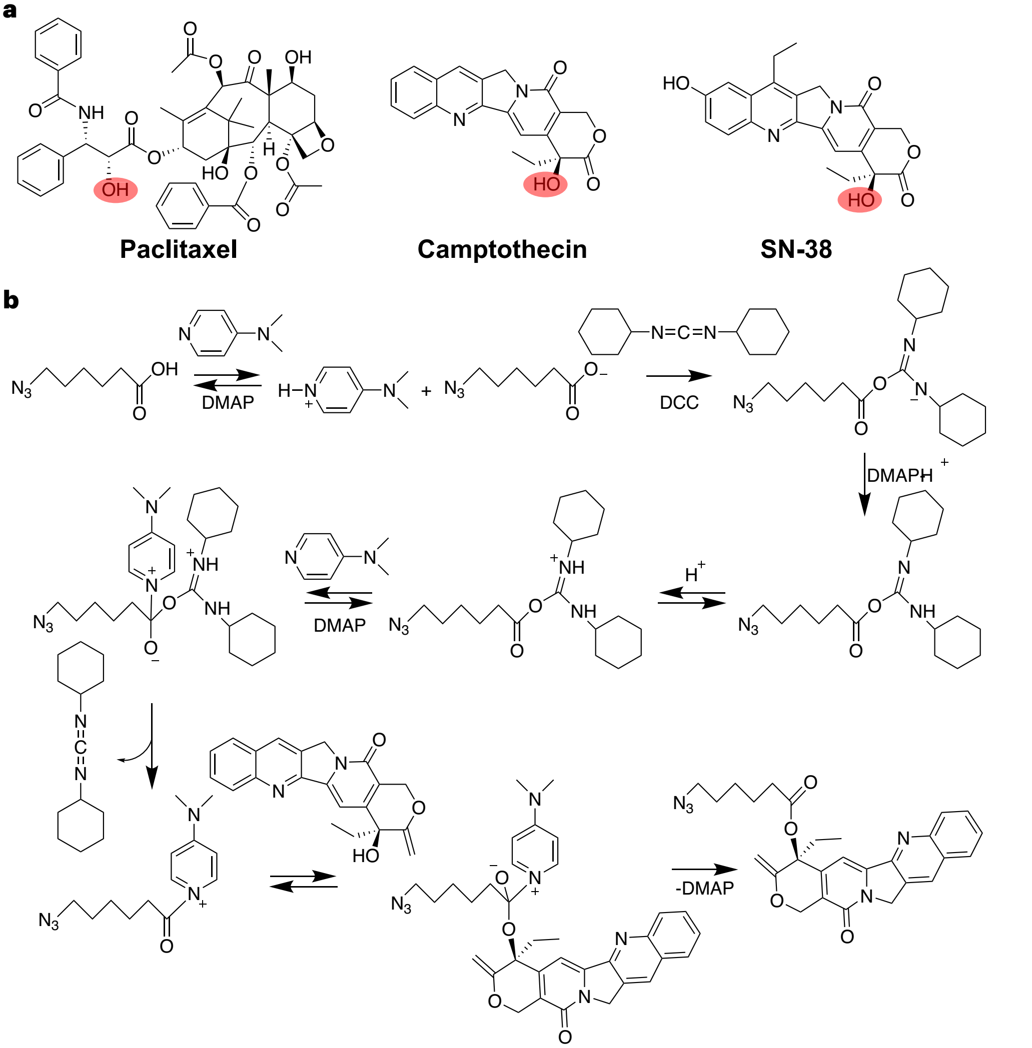

Fig. 4 | Synthesis scheme of chemical drug modification into prodrugs via Steglich esterification. **a**, Chemical structure of chemotherapeutic drugs used for esterification reaction, with the most reactive hydroxyl sites highlighted in red. **b**, Chemical reaction scheme of the esterification reaction of CPT as a model. DMAP, 4-dimethylaminopyridine.

liquid chromatography (HPLC) or polyacrylamide gel purification. Desalting (described in the Procedure) provides the fastest procedure but at the cost of your RNA product containing some aborted strand contaminants; on the other hand, HPLC and gel purification are more time consuming but will provide RNA products of the exact desired size and thus sequence. Because of the optimal length and high affinity of the 4WJ component strands toward each other, the aborted strands are generally incorporated at a relatively low rate due to lowered affinity with other 4WJ strands.

In addition, the desired chemotherapeutic must be selected. In this protocol, the conjugation of PTX[41,64], CPT[42] and SN38 (refs. 43,44) is demonstrated (Fig. 4a). All of these chemotherapeutics are highly effective in inhibiting cell growth, including of many cancer cell types, and have been used in the clinic but have lost favor because of their limitations discussed above[100–104]. These drugs were also selected because they have a hydroxyl group that can be modified to generate a prodrug with an azide. The chemotherapeutic prodrugs were generated by Steglich esterification combining each of the chemotherapeutics with a 6-azidohexanoic acid to generate an azide linker[42,105] (see Fig. 4b for the reaction scheme). The selection of

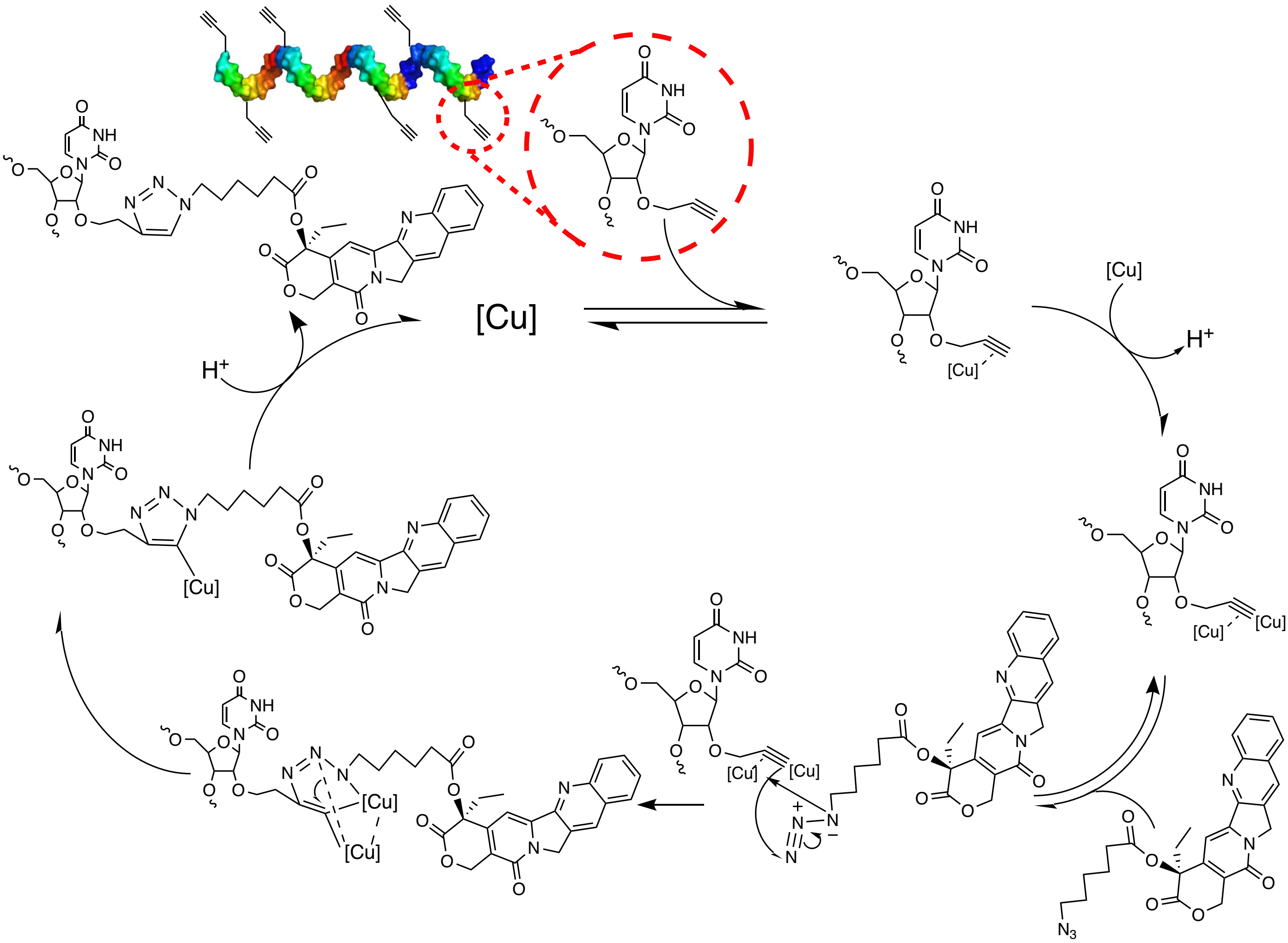

Fig. 5 | Synthesis scheme of drug conjugation to the RNA oligo using copper-chelated click chemistry. Shown here is the SN-38 prodrug-conjugated RNA oligo with six alkyne modifications.

an ester linker provides a stimuli-sensitive linker that is aimed to release the chemical drug in the presence of tumor esterases and return the prodrug back to its original structure. This prodrug is then purified by silica column and characterized by mass spectroscopy, thin-layer chromatography and nuclear magnetic resonance (NMR) to ensure that the Steglich esterification reaction takes place and quantify the relative yield of the reaction. The synthesized RNA oligos are then reacted with these chemotherapeutic prodrugs under copper-chelated click chemistry to link the azide to the RNA-alkyne[41,42] (Fig. 1). Copper-chelated click chemistry allows for a simple and fast reaction for a high yield of drug conjugation to RNA. In addition, click chemistry uses biological molecules in a single reaction step (reaction scheme shown in Fig. 5). After conjugation, the RNA strands are purified to remove excess unconjugated drug and copper via reverse-phase HPLC or polyacrylamide gel electrophoresis and characterized for drug incorporation.

The final stage of the Procedure is the assembly of the RNA nanoparticle from each of its component strands (Fig. 1) and testing the delivery of the chemotherapeutic by the RNA nanoparticle. The 4WJ is assembled from the four strands followed by characterization to ensure the assembly, size and stability of the nanoparticle[41]. The RNA nanoparticles should be characterized for thermostability, enzymatic stability, drug-release profiles and nanoparticle size and charge characterization. The RNA nanoparticle drug conjugate is then tested in in vitro and in vivo cancer models to ensure safety and tumor inhibition. It is expected that the chemotherapeutic is released via the ester bond by either tumor esterases or water hydrolysis and returned to its original structure with the hydroxyl group.

Comparison of alternative methods

The concept of delivering toxic chemical drugs such as chemotherapeutics has been a long-term goal of nanotechnology[106]. Numerous nanoparticle material platforms that have loaded chemotherapeutics for the delivery to solid tumors have been developed. Below we discuss several alternative nanoparticle platforms.

Liposomes

Since their discovery in 1965, liposomes, a class of lipid-based nanoparticles, have been used to deliver various therapeutic cargoes through encapsulation into either the lipid bilayer or aqueous core[107,108]. Liposomes are primarily made up of phospholipids and include cholesterol, which is essential for the particle formation and stability[108,109]. Liposomes commonly also include PEGylated (PEG, polyethylene glycol) lipids to aid in stability and improve biodistribution profiles to aid in drug delivery. Loading of drugs is achieved by encapsulation during the formation of liposomes, and various therapeutics can be loaded into their core, including hydrophilic drugs, RNAs, DNA or proteins[109], while hydrophobic drugs can be loaded into the lipid bilayer[110–112]. Theoretically, liposomes can range from 20 to 1,000 nm in size[108] but are typically larger in size (<100 nm) compared to RNA nanoparticles, which can cause macrophage phagocytosis, endoplasmic reticulum stress and biodistribution challenges because of lipids' ability to pass through the cell membrane of healthy cells, as demonstrated by high levels of accumulation in healthy organs[113–115]. Liposomes on their own rely on passive tumor targeting, unless functionalized with ligands through additional assembly steps, thus limiting tumor accumulation and delivery to targeted cells[116]. However, they benefit from being biodegradable, making them relatively safe, and are able to release therapeutics without endosome trapping[110]. As a result, chemotherapeutics encapsulated in liposomes result in extended circulation time and extended release of drugs and are currently used in the clinic[117].

Polymer-based nanoparticles

Both simple and highly complex polymeric nanoparticles involving several polymers and layers have been designed[118–121]. Polymeric nanoparticles can be composed of various polymers but commonly use poly(lactic-co-glycolic acid) and are functionalized with PEG. They are highly tunable for defined stability based on the polymers used and can vary in characteristics such as size, surface charge and drug loading. Polymer nanoparticles inherently do not have cell-specific targeting but have been modified to include tumor-targeting ligands[118,119]. Overall, polymer nanoparticles can suffer from homogeneity issues, accumulation in healthy organs due to their larger size and lack of biocompatibility[118,122]. Yet, polymer nanoparticles have shown promise in shielding the loaded drug to prevent cytotoxicities and better solubilize drugs.

Inorganic nanoparticles

Inorganic nanoparticles make up a wide range of nanoparticles including iron oxide nanoparticles, ceramic nanoparticles and titanium, gold, silica and silver nanoparticles[122–124]. These nanoparticles typically comprise a solid core with functionalization on the exterior. These nanoparticles are commonly signal responsive, for example, to photothermal therapy or are photoresponsive at the delivery environment[124]. This provides a precise release of therapeutics at the desired site, but inorganic nanoparticles often come with high accumulation in the lung, liver and kidneys; require surface modifications for improved biodistribution[125]; and result in toxicities.

Albumin-based nanoparticles

Albumin is a natural ligand-carrying protein in the blood that has been used to load chemotherapeutics[126–128]. The most notable albumin–drug complex is Abraxane (or nab-PTX)[129,130], a PTX-loaded nanoparticle that enhances drug solubility. Albumin nanoparticles also vastly prolong the half-life of rapidly cleared drugs by increasing the size of the chemical drugs to improve biodistribution. They are able to load high loads of drugs into a single protein[126]. However, the lack of effective tumor targeting has limited albumin nanoparticles, and there is now criticism that Abraxane is unable to improve the toxicity and side-effects of PTX, putting its effectiveness in question[131,132].

ADCs

ADCs have boomed onto the market, with nearly 100 entering clinical trials[133], for their ability to provide on-target delivery of conjugated chemotherapeutics[7,8,134]. ADCs are engineered monoclonal antibodies that have been designed to bind to an overexpressed receptor on tumors to allow for active tumor targeting while carrying chemotherapeutics that are conjugated through linkers similar to those used on RNA nanoparticles. In addition, ADCs can provide a secondary therapeutic response through receptor inhibition on the tumor cells[133]. The construction of ADCs requires several steps that make their production complex compared to other nanotechnology platforms. The amphophilic nature and bulky size of ADCs can result in nonspecific cell binding and unfavorable biodistribution. However, their efficacy outweighs these negatives. Furthermore, a current challenge in the ADC field is overcoming toxicities, such as central nervous system toxicity, hypersensitivity reactions and immune responses[10,133]. These may be related to ADCs being proteins and thus eliciting immune responses and to issues with homogeneity and stability of drug conjugates.

Other nucleic acid nanotechnology

Nucleic acid nanoparticles can be composed of DNA or RNA. Both share some of the principles in nanoparticle construction and assembly and can be fabricated into similar architectures[135,136]. However, there are some significant differences between DNA and RNA concerning thermostability, folding principles, ion requirements for assembly and in vivo behavior. DNA nanotechnology uses mainly Watson–Crick base-pairing for structure folding and assembly, whereas RNA technology also uses non-canonical base-pairing to add further structure diversity, stability, motility and deformability. Both DNA and RNA can produce branched motifs that allow for the generation of origami through intermolecular interactions[136,137]. DNA provides similar tunability and programmable design to RNA to produce wire-framed DNA nanoparticles that have been explored as drug-delivery vehicles[138]. The use of DNA aptamers can provide DNA nanoparticles with the needed active targeting of tumor cells, and studies have demonstrated the in vitro feasibility to deliver gene silencing therapeutics and intercalated chemical drugs (i.e., doxorubicin)[138–140]. However, DNA architectures have a lower thermodynamic stability than RNA architectures and generally require a minimum of 10 mM magnesium ions for nanoparticle folding into a stable structure[49,138], whereas the magnesium concentration in vivo is lower than the 10 mM needed. In addition, DNA nanoparticles must address, through careful design, sensitivity to nucleases because double-stranded DNA is stable because the human body lacks double-stranded DNA degradation enzymes, but single-stranded DNA is sensitive to the single-stranded DNase degradation that takes place in vivo. DNA nanoparticles have successfully conjugated PTX; however, designs were limited to one molecule per DNA strand[141,142]. This limits the drug-loading capacity compared to the six conjugated drugs per strand on the RNA 4WJ and would require a more intricate DNA nanoparticle design to reach a higher number of drug molecules per nanoparticle. Conjugation of multiple chemotherapeutics per oligo would destabilize the DNA nanoparticles much like in the less thermostable RNA 3WJ nanoparticle compared to the RNA 4WJ[41].

The 4WJ nanoparticle described in this protocol relies on base pairing to form its highly stable singular structure, compared to other RNA nanoparticle platforms that assemble from multiple subunits into nano-complexes through intermolecular kissing loops or bulge interactions, such as tectoRNA, and sticky ends[69,143]. These strategies have generated several RNA nanoparticles into 2D nanostructures, 3D prisms and nanoarrays[62,67,90,93,143–146]. RNA nanoparticles of more complex design[54,60,87,94,147–150] with a size larger than the 4WJ may have the ability to allow for drug conjugation and may increase drug loading over the 4WJ; however, changes in particle size and shape greatly influence biodistribution, toxicity and immunostimulant properties[38,44,51]. Further studies of other larger and more complex RNA nanoparticles would have to be conducted to evaluate and optimize their anti-tumor-to-toxicity profiles.

Advantages and limitations

RNA is an anionic polymer[21,151–155] that holds two unique properties: structurally, it is thermostable with high T_m values, while conformationally, it is dynamic[154,156,157] and deformable[153,158]. RNA as a biopolymer with a unique base-pairing nature and its charged backbone leads to the following structuring particularities: near-neighbor principles[159–161], strand breathing[21,162], pseudoknot formation[163–165], induced fit[166–168] and conformation capture[169–171]. Thus, RNA is motile, dynamic[154,156,157], deformative[20,21], elastic[20,172,173] and a primitive living material[174–176]. Its anionic nature prevents its nonspecific entry into healthy cells that also have a negatively charged lipid membrane, resulting in repulsion by electrostatic charges. These advantages of RNA contribute to its spontaneous and high efficiency tumor targeting, with fast excretion from the body without toxicity. RNA nanoparticles are advantageous for the delivery of therapeutics to solid tumors, as demonstrated across several tumor models including colorectal cancer[43,74,177], triple negative breast cancer (TNBC)[32,33,50], non-small-cell lung cancer[31], prostate cancer[29], ovarian cancer[178,179], glioblastoma[72,76] and gastric cancer[73]. RNA is dynamic; thus, it undergoes restructuring events generating motion and wobble[20]. When developed into nanoparticles, RNA assembles into defined shapes but retains its dynamic property[21,46]. It was also shown that RNA nanoparticles are elastic[20], in that they deform under external forces and return to their native structure upon relaxation of forces. These dynamic and deformable properties allow the RNA nano-scaffolds to slip through the actively growing blood capillaries in tumor vasculature. In addition, these properties result in rapid renal excretion via the 5.5-nm glomerular filter, preventing interactions and accumulation in healthy organs[20,49]. Thus, RNA nanoparticles provide a beneficial biodistribution profile, with >5% of injected dose accumulating in the tumor environment without showing long-term accumulation in healthy organs or pathological change to these tissues[39,41,44]. The immunogenicity of RNA nanoparticles is shape, size, sequence and stoichiometry dependent[52,180]. RNA nanoparticles can thus be modified to serve as immune adjuvants[51] or can be designed as the 4WJ, which does not induce an immune response[44]. As such, these nanoparticles have proven to be a safe delivery vehicle for previously poorly tolerated chemotherapeutics. In addition, RNA nanoparticles allow for the combination delivery of therapeutics such as chemical drugs with miRNA[34] or multiple chemotherapeutics (such as gemcitabine and SN38) to result in synergistic inhibition of tumors[43] (Fig. 6).

Although RNA nanoparticles provide numerous benefits and are an ideal drug-delivery vehicle, the number of RNA nanoparticles translating into the clinic is currently limited.

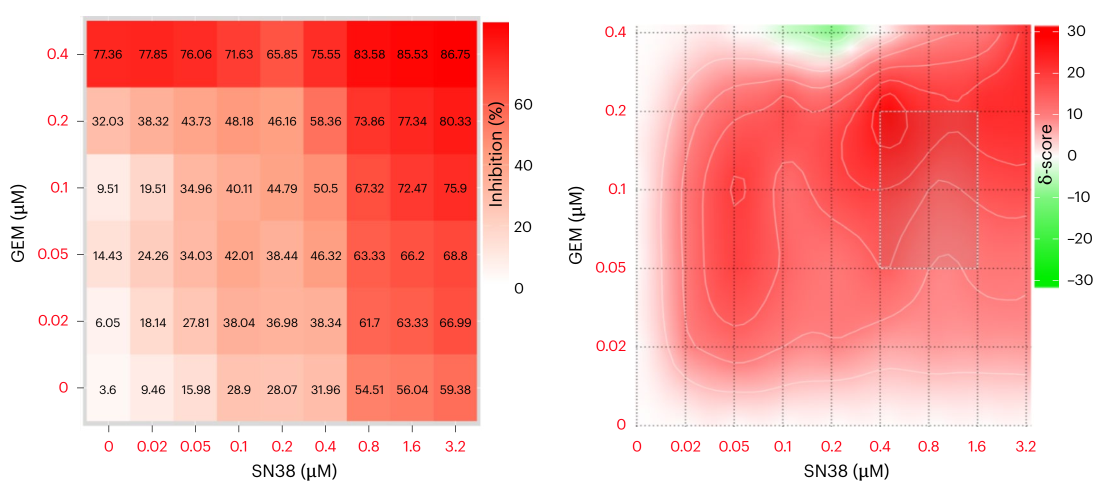

Fig. 6 | Combinational delivery of SN38 and gemcitabine chemotherapies achieved by 4WJ RNA nanoparticles. Dose–response matrix of 4WJ-GEM/SN38 and highest single agent synergy map of 4WJ conjugated with gemcitabine (GEM) and SN38. Adapted with permission from ref. 43, Elsevier.

One of the largest limitations of RNA nanotechnology was the scalability in production and its related cost of synthesis[19,21,181,182]. The challenge of cost has been resolved by the industrial RNA production at good manufacturing practices grade. Industrial scaling of RNA production can now produce gram- or kilogram-scale batches of RNA complex. Because of the 98.5% efficiency limit of nucleotide incorporation, solid-phase synthesis of RNA is limited to 120 nt in length to ensure the yield of the full-length RNA in the final products. This can limit the design of RNA nanoparticles to maximize drug loading, because approximately 5-nt spacing between drug conjugation sites is required to prevent drug aggregation[41]. A possible solution is to produce RNA dendrimers[58,183], 6WJs[34] or larger RNA nanoparticles, similar to replacing a large Lego brick with several smaller pieces having the same overall footprint. However, for solid tumor therapy, production of larger RNA complexes will introduce the problem of unfavorable biodistribution due to macrophage engulfment[38,184]. Currently, production of RNA nanoparticles with alkyne modifications cannot be done via in vitro transcription using T7 RNA polymerase because 2′-propargyl-modified triphosphate nucleotides are not commercially available. However, in the future, these nucleotides could be produced and incorporated into long RNA oligos by mutant T7 RNA polymerases. Currently, each strand comprising the 4WJ is about 40 nt, and incorporation of most RNA aptamers remains within the capabilities of solid-phase synthesis.

To improve this technique, enhanced RNA-folding models need to be developed. The field of RNA folding is progressing in predicting RNA structures, as shown with the release of AlphaFold 3 (ref. 185), RNAComposer[95,186] and Rosetta and trRosettaRNA[187,188] for predicting RNA structure[189]. Finally, the longstanding concern over RNA instability in circulation and susceptibility to RNases has been solved by the use of 2′-nucleotide modifications, such as 2′-fluorine or 2′-*O*-methyl[49,190,191]. Such modifications, as well as the 2′-propargyl modification used here, allow for RNA nanoparticles to remain stable in the presence of serum RNases for >36 h[41,190].

Experimental design

Here, we discuss the design criteria for generating stable RNA nanoparticles that allow for the conjugation of chemotherapeutics without destabilizing the nanoparticles, preventing drug aggregation and loading enough drug for strong therapeutic response.

RNA nanoparticle design

In this protocol, we describe the conjugation of PTX, CPT and SN38 to our developed 4WJ RNA nanoparticle[41–43]. This protocol is highly adaptable, and the experimental design can be varied. In the design of the RNA nanoparticle, one must consider the cancer type being targeted, the chemotherapeutic to be conjugated, the possible combination with iRNA components and the nanoparticle itself[34]. Any RNA nanoparticle can be used, as long as it includes the 2′-propargyl modifications and demonstrates high enough stability, as discussed above. The folding and thermodynamic stability of a nanoparticle can be modeled through computational modeling or experimental testing before following this protocol, to ensure a T_m > 70 °C[192–198]. In addition, because of the variety of modified phosphoramidites, this protocol can be adapted to use other desired chemicals for linking chemical drugs to the RNA sugar chain.

Selection of targeting ligand for specific tumor types

The features of the targeted tumor or cell type are of importance for selecting a targeting ligand. RNA aptamers, DNA aptamers and chemical ligands have all previously been used on RNA nanoparticles and allow for the targeting of specific receptors on tumor cells[29,31–33,43,50,72–74,76,177–179]. For example, EGFR has been shown to be over-expressed on several tumors including TNBC[32,199] and non-small-cell lung cancer[31,200], and the inclusion of an EGFR-binding aptamer has allowed for specific targeting of these tumors by RNA nanoparticles. Prostate-specific membrane antigen is over-expressed in prostate cancer subtypes and has become a popular receptor to target because of the high affinity of its RNA aptamer[201–203]. Any tumor type can be targeted by RNA nanoparticles with the vast library of available ligands[204]. The modularity and adaptability of RNA nanoparticles allow for the exchange of targeting ligands to the desired target.

Selection of chemotherapeutics for conjugation

There is a wide variety of chemotherapeutics and anti-cancer chemical drugs on the market that can be used for conjugation into RNA nanoparticles. Many of these can be substituted into the RNA nanoparticle over the described PTX, CPT and SN38. The total number of drug conjugates can be controlled through the number of 2′-propargyl modifications included on each RNA oligo strand. If fewer modifications are included, the total number of chemotherapeutic molecules will decrease per RNA nanoparticle and may result in decreased anti-tumor effects and limit nanoparticle performance. In addition, the number of 2′-propargyl–modified nucleotides can be increased; however, they should be spaced by ≥5 nt. Closer spacing can lead to nanoparticle destabilization and aggregation of the chemical drug. If this occurs, RNA nanoparticles will not remain stable in vivo, resulting in off-target delivery, and drug aggregates will not be covalently linked to the RNA nanoparticle, which will result in early release during circulation. RNA nanoparticles are highly adaptable, but the design parameters must be carefully tuned to ensure desired results.

Conjugating additional molecules to RNA nanoparticles

Furthermore, additional chemicals of interest can be conjugated to the RNA nanoparticle, not just chemotherapeutics. To directly follow the protocol here, a chemical must have a hydroxyl (-OH) group that is readily reactive for the addition of the azidohexanoic acid linker through Steglich esterification[105]. However, many additional chemical reactions can be used for other chemicals, such as *N*-hydroxysuccinimide (NHS) ester chemistry to add an azido linker to a chemical or drug to be conjugated. NHS ester chemistry would allow the conjugation of a drug with a primary amine to click onto an RNA nanoparticle, vastly diversifying the number of chemicals that can be used to modify the RNA oligos. One must take into consideration the release of the chemical or drug from the RNA nanoparticle and its ability to return to its original structure and function. To that end, nucleic acid nanoparticles (DNA and RNA) have used several stimuli-responsive linkers to conjugate chemical drugs to the nanoparticles[41,142,205–207]. Prodrug release has been designed through linkers that are tumor sensitive via changes in pH (i.e., hydrazone or imine), hypoxia (i.e., azobenzene) and reactive oxygen species (i.e., thioketal). In addition, linkers have been designed to be cleaved by tumor-associated enzymes such as esters, peptides and L-γ-glutamylglycine as well as glutathione-responsive linkers such as disulfide linkers that are responsive in the extracellular matrixes of tumors. These linkers have been well reviewed by others and can be adapted into RNA nanoparticles through the generation of prodrugs[208–211].

Expertise needed to implement the protocol

The conjugation of chemotherapeutics to RNA nanoparticles combines concepts and procedures from several scientific disciplines, including nucleic acid chemistry, organic chemistry, analytical chemistry and molecular biology, and the testing of the nanoparticles requires cellular biology and animal care skills. With that said, the procedures detailed can be followed by a competent graduate student, postdoctoral researcher or similar. If the researcher lacks skills or training in an individual part of the protocol, many research institutes provide core facilities that can be used.

Regulatory approvals

The procedures described involve several health risks that must receive regulatory approvals before completing the experiments. Some institutes have safety considerations for the generation and manipulation of nanoparticle materials. Although RNA nanoparticles generally do not fall into a nanoparticle hazard, compared to graphene, heavy metals or polymer-based particles, it is still important to check the required approval status of RNA nanoparticles. In addition, RNA nanoparticles, depending on the institute, may fall under recombinant nucleic acid safety requirements. RNA nanoparticle sequences do not match any gene in the human body and are fully synthetic, so they are often exempt from these regulations. The testing of the RNA nanoparticles in cell lines will require the institutional biosafety committee, or similar, review before completing experiments. These procedures have previously been approved by the University of Kentucky and The Ohio State University's Institutional Biosafety Committee, and one can expect the approval process to take 1–3 months.

Materials

Biological materials

▲ **CAUTION** The cell lines used in your research should be regularly checked to ensure that they are authentic and are not infected with mycoplasma.

- MDA-MB-231 human breast cancer cells (American Type Culture Collection, cat. no. HTB-26; RRID: CVCL_0062)
- RAW 264.7 mouse macrophage cells (American Type Culture collection, cat. no. TIB-71; RRID: CVCL_0493)

Reagents

▲ **CAUTION** All phosphoramidites are moisture sensitive and reactive in water. All phosphoramidites should be freshly dissolved in anhydrous acetonitrile (ACN) and be opened only in a moisture-free environment, such as dried argon in a chemical glove box. Dissolved phosphoramidies should be disposed of after 3 d of storage in an argon atmosphere.

▲ **CRITICAL** Unless specified, all the reagents can be replaced with other brands, if available.

- (*S*)-(+)-CPT (Sigma-Aldrich, cat. no. PHL89593)
  ▲ **CAUTION** CPT is toxic if swallowed and may cause genetic defects. Wear gloves and goggles when handling.
- 1-Ethyl-3-(3-dimethylaminopropyl) carbodiimide hydrochloride (EDC; Thermo Scientific, cat. no. 22980)
  ▲ **CAUTION** EDC is moisture sensitive. It may cause eye and skin irritation. Wear gloves and goggles when handling.
- 2′-tBDsilyl adenosine (n-bz) β-cyanoethyl *N*,*N*-diisopropyl (CED) phosphoramidite (Chemgenes, cat. no. ANP-5671)
  ▲ **CAUTION** 2′-tBDsilyl adenosine (n-bz) CED phosphoramidite is moisture sensitive.
- 2′-tBDsilyl cytidine (n-acetyl) CED phosphoramidite (Chemgenes, cat. no. ANP-6676)
  ▲ **CAUTION** 2′-tBDsilyl cytidine (n-acetyl) CED phosphoramidite is moisture sensitive.
- 2′-tBDsilyl guanosine (n-ibu) CED phosphoramidite (Chemgenes, cat. no. ANP-5673)
  ▲ **CAUTION** 2′-tBDsilyl guanosine (n-ibu) CED phosphoramidite is moisture sensitive.
- 2′-tBDsilyl uridine CED phosphoramidite (Chemgenes, cat. no. ANP-5674)
  ▲ **CAUTION** 2′-tBDsilyl uridine CED phosphoramidite is moisture sensitive.
- 2′-Fluoro-2′-deoxy cytidine (n-ac) CED phosphoramidite (Chemgenes, cat. no. ANP-9152)
  ▲ **CAUTION** 2′-Fluoro-2′-deoxy cytidine (n-ac) CED phosphoramidite is moisture sensitive.
- 2′-Fluoro-2′-deoxy uridine CED phosphoramidite (Chemgenes, cat. no. ANP-9154)
  ▲ **CAUTION** 2′-Fluoro-2′-deoxy uridine CED phosphoramidite is moisture sensitive.
- 2′-*O*-Propargyl cytidine (n-bz) CED phosphoramidite (Chemgenes, cat. no. ANP-7752)
  ▲ **CAUTION** 2′-*O*-Propargyl cytidine (n-bz) CED phosphoramidite is moisture sensitive.
- 2′-*O*-Propargyl uridine CED phosphoramidite (Chemgenes, cat. no. ANP-7754)
  ▲ **CAUTION** 2′-*O*-Propargyl uridine CED phosphoramidite is moisture sensitive.
- 3% (vol/vol) trichloroacetic acid (TCA) in dichloromethane (Fisher Scientific, cat. no. 40-4140-62)
  ▲ **CAUTION** TCA in dichloromethane causes serious eye damage, is suspected of causing cancer and causes skin irritation. Wear gloves and goggles and dispense it in a vented hood.
- 4-(Dimethylamino)pyridine (Sigma-Aldrich, cat. no. 107700)
  ▲ **CAUTION** 4-(Dimethylamino)pyridine causes serious acute toxicity and damage to organs through oral contact, inhalation and skin contact. Wear gloves and goggles and dispense it in a vented hood.
- 40% (wt/vol) aqueous methylamine (Sigma, cat. no. 426466-100ML)
  ▲ **CAUTION** Methylamine solution is highly flammable and harmful through skin contact or if swallowed or inhaled. Wear gloves and goggles and dispense it in a vented hood.
- 5′-Hexynyl phosphoramidite (Glen Research, cat. no. 10-1908-02E)
- 5′-Amino-modifier (Glen Research, cat. no. 10-1906-02E)
- 6-Azidohexanoic acid (Chem-IMPEX, cat. no. 29363)

- Acetic acid, glacial (HAc, Fisher, cat. no. A38C-212)
▲ **CAUTION** HAc is a weak acid; it is corrosive and is a skin, eye and respiratory tract irritant. Wear gloves and goggles and dispense it in a vented hood.
- ACN (HPLC grade) (Fisher, cat. no. A998SK-4)
▲ **CAUTION** ACN is highly flammable, can cause serious eye irritation and is harmful if swallowed. Wear gloves and goggles.
- ACN, anhydrous (Fisher Scientific, cat. no. BP1170-4)
▲ **CAUTION** ACN is highly flammable, can cause serious eye irritation and is harmful if swallowed. Wear gloves and goggles.
- Acrylamide, ≥99%, electrophoresis grade (Acros Organics, cat. no. 164850025)
▲ **CAUTION** Acrylamide may cause cancer and heritable genetic damage. It is harmful by inhalation and in contact with skin. It is toxic if swallowed. Wear gloves and a mask.
- Acrylamide/Bis 40% (wt/vol) solution, acrylamide/bis-acrylamide ratio 29:1 (Fisher, cat. no. BP1408-1)
▲ **CAUTION** Acrylamide is highly toxic and is a carcinogen. Wear gloves and goggles.
- Activator, 0.25 M 5-ethylthio-1H-tetrazole in anhydrous ACN (Sigma, cat. no. L030000-6X450ML)
▲ **CAUTION** 5-Ethylthio-1H-tetrazole causes severe skin burns and eye damage and may cause respiratory irritation. Wear gloves and goggles.
- Alexa Fluor 488 phalloidin (ThermoFisher Scientific, cat. no. A12379)
▲ **CAUTION** Alexa Fluor 488 phalloidin can cause acute toxicity if swallowed, if it comes in contact with skin or if it is inhaled. Wear gloves and goggles and dispense it in a vented hood.
- Ammonium acetate (NH_4OAc; J.T. Baker, cat. no. 0596-01)
- Ammonium carbonate (Sigma, cat. no. 207861-25G)
- Ammonium hydroxide solution (Sigma, cat. no. 05003-1L)
▲ **CAUTION** Ammonium hydroxide causes severe skin burns, eye damage and respiratory irritation. Wear gloves and goggles.
- Ammonium persulfate (APS; Fisher, cat. no. BP179-100)
▲ **CAUTION** APS is harmful if swallowed and causes skin irritation and serious eye irritation. Wear gloves and goggles and dispense it in a vented hood.
- Bis-acrylamide (Fisher, cat. no. BP171-100)
▲ **CAUTION** Bis-acrylamide causes eye, skin and respiratory tract irritation. It is harmful if inhaled, swallowed or absorbed through the skin. It may cause central nervous system effects. Wear gloves, goggles and a mask.
- Boric acid (Fisher, cat. no. A74-500)
▲ **CAUTION** Boric acid may damage fertility and the fetus during pregnancy.
- Bromophenol blue (Sigma, cat. no. B-8026)
▲ **CAUTION** Bromophenol blue is a skin and respiratory tract irritant.
- Capping reagent A - tetrahydrofuran (THF)/lutidine/acetic anhydride (8:1:1) (Bioautomation, cat. no. BIO221/0450)
- Capping reagent B - 16% (vol/vol) n-methylimidazole in THF (Bioautomation, cat. no. BIO345/0450)
- CellTiter 96 non-radioactive cell proliferation assay (Promega, cat. no. G4000)
- Clorox regular bleach (VWR, cat. no. 37001-058)
▲ **CAUTION** Bleach is corrosive and can cause severe irritation or damage to eyes and skin. It is harmful if swallowed.
- Copper(I) bromide (CuBr; Sigma-Aldrich, cat. no. 212865)
▲ **CAUTION** CuBr causes skin irritation and eye damage and is harmful if swallowed. Wear gloves and goggles.
- Cystamine dihydrochloride, 97% (Acros Organics, cat. no. 111770250)
▲ **CAUTION** Cystamine causes eye, skin and respiratory tract irritation. It may be harmful if swallowed, inhaled or absorbed through the skin. Wear gloves, a mask and goggles.
- Deuterated chloroform (Cambridge Isotope Laboratories Inc., cat. no. DLM-7-10X0.6)
▲ **CAUTION** Deuterated chloroform causes skin irritation and eye damage. Wear gloves and goggles.

- Dichloromethane, anhydrous (Fisher Scientific, cat. no. AC348460025)
  ▲**CAUTION** Dichloromethane causes skin irritation and eye damage. Wear gloves and goggles.
- Diethyl pyrocarbonate (DEPC; Sigma, cat. no. D-5758)
  ▲**CAUTION** DEPC causes acute oral toxicity. Wear gloves.
- 4-Dimethylaminopyridine (ThermoFisher Scientific, cat. no. 148270250)
- Dimethyl sulfoxide (DMSO; Acros Organics, cat. no. 348445000)
  ▲**CAUTION** Avoid contact with skin and eyes.
- DMEM (ThermoFisher Scientific, cat. no. 11965092)
- DMEM/F-12 medium (ThermoFisher Scientific, cat. no. 11320033)
- EDTA disodium salt, dihydrate (Sigma, cat. no. E-5134)
  ▲**CAUTION** EDTA is a skin, eye and respiratory tract irritant.
- Ethanol, 100% (Pharmco-AAPER, cat. no. 111000200)
  ▲**CAUTION** Ethanol is a flammable liquid.
- Ethidium bromide (Fisher, cat. no. P1302-10)
  ▲**CAUTION** Ethidium bromide is a strong carcinogen; it is a skin, eye and respiratory tract irritant. Wear gloves and dispense it in a chemical hood.
- Ethyl acetate (J.T. Baker, cat. no. 9280-03)
  ▲**CAUTION** Ethyl acetate causes skin irritation and eye damage. Wear gloves and goggles.
- Ethylenediamine dihydrochloride (Thermo Scientific, cat. no. 23031)
  ▲**CAUTION** Ethylenediamine may cause eye, skin and respiratory tract irritation. It may be harmful if swallowed, inhaled or absorbed through the skin. Wear gloves, a mask and goggles.
- exACT gene 50-bp mini DNA ladder (Fisher, cat. no. BP2570100)
- Fetal bovine serum (FBS), heat inactivated (Sigma, cat. no. F4135)
- Fluorescein isothiocyanate (FITC) annexin V apoptosis detection kit (BD Pharmingen, cat. no. 556570)
- Formamide (Fisher, cat. no. F84-1)
  ▲**CAUTION** Formamide is harmful if swallowed, inhaled or absorbed through the skin. It causes eye and skin irritation. It may cause respiratory tract irritation, affect the central nervous system and cause liver damage. Wear gloves.
- Glen Gel-Pak 2.5 desalting column (Glen Research, cat. no. 61-5025-25)
- Hydrochloric acid (HCl; Fisher, cat. no. A144-212)
  ▲**CAUTION** HCl is a strong acid; it is very corrosive and is a skin, eye and respiratory tract irritant. HCl can cause severe burns. Wear gloves and goggles and dispense it in a vented hood.
- Magnesium chloride hexahydrate ($MgCl_2$; Fisher, cat. no. M33-500)
- Methanol (Fisher, cat. no. A412-4)
  ▲**CAUTION** Methanol is a dangerous, poisonous and flammable liquid and vapor. It is harmful if inhaled. It may be fatal or cause blindness if swallowed. It may cause eye and skin irritation. It may cause central nervous system depression, kidney damage and reproductive and fetal effects. Wear gloves and goggles and dispense it in a vented hood.
- Milli-Q water, 18.2 MΩ cm^{-1} resistivity
- Molecular trap (Bioautomation, cat. no. BG7-0013-1)
- Mouse ELISA MAX deluxe sets (BioLegend, cat. no. 433404)
- Mouse IFN-α ELISA kit (R&D Systems, cat. no. MFNAS0)
- *n*-Hexane (C_6H_{14}; Mallinckrodt Chemicals, cat. no. 5189-08)
  ▲**CAUTION** *n*-Hexane is a flammable liquid and causes skin irritation and eye damage. Wear gloves and goggles.
- *N*,*N*′-Dicyclohexycarbodiimide (Acros Organics, cat. no. AC113901000)
- Opti-MEM reduced serum medium (Thermo Fisher, cat. no. 31985062)
- Oxidizer, 0.02 M iodine in tetrahydrofuran/pyridine/water (70:20:10) (Sigma, cat. no. L260045-06)
  ▲**CAUTION** Iodine in tetrahydrofuran/pyridine/water is a highly flammable liquid and vapor. It is harmful if swallowed or if it comes in contact with the skin. It causes skin irritation and serious eye irritation. Wear gloves and goggles and dispense it in a vented hood.

- PTX (ThermoFisher Scientific, cat. no. J62734.ME)
  ▲ **CAUTION** PTX causes skin irritation and serious eye damage and may cause respiratory irritation. Wear gloves and goggles and dispense it in a vented hood.
- Paraformaldehyde (4% (wt/vol); Biotium, cat. no. 22023)
  ▲ **CAUTION** Paraformaldehyde is a flammable solid. It is harmful if swallowed or if it comes in contact with the skin. It causes skin irritation and serious eye irritation. Wear gloves and goggles and dispense it in a vented hood.
- Penicillin-streptomycin (0.25% (wt/vol); Gibco by Life Technologies, cat. no. 15070-063)
- Phosphate-buffered saline (PBS) (pH 7.4; Thermo Fisher, cat. no. 10010023)
- Prolong gold antifade reagent with DAPI (Life Technologies, cat. no. P36935)
- RediSep empty disposable sample load cartridges, 65-gram hold (Teledyne ISCO, cat. no. 69-3873-225)
- RediSep silver silica gel disposable flash columns, 12-gram (Teledyne ISCO, cat. no. 69-2203-312)
- Silica gel, 60–200 mesh (SiO_2; Milipore Sigma, cat. no. SX0143U-1)
  ▲ **CAUTION** Silica gel causes eye damage and may cause respiratory irritation. Wear gloves and goggles and dispense it in a vented hood.
- SN38 (7-ethyl-10-hydroxycamptothecin; Sigma, cat. no. H0165)
  ▲ **CAUTION** SN-38 is harmful if swallowed, causing acute toxicity, reproductive toxicity and specific target organ toxicity. Wear gloves and goggles.
- Sodium acetate trihydrate (NaOAc; Fisher, cat. no. S209-3)
- Sodium bicarbonate ($NaHCO_3$; Millipore Sigma, cat. no. S5761-500G)
- Sodium chloride (NaCl; Fisher, cat. no. S271-500)
- Sodium dodecyl sulfate (SDS; Fisher, S529-500)
  ▲ **CAUTION** SDS is an eye and respiratory tract irritant.
- Sodium hydroxide (NaOH; Fisher, cat. no. S318-3)
  ▲ **CAUTION** NaOH is corrosive and can cause chemical burns. Wear gloves, a laboratory coat and eye protection when handling the material or its solutions. Dissolution of NaOH is highly exothermic, and the resulting heat may cause heat burns or ignite flammables. It also produces heat when reacted with acids.
- Sodium sulfate, anhydrous (Na_2SO_4; Macron Fine Chemicals, cat. no. MFCD00003504)
- Sucrose (Fisher, cat. no. S5-3)
- Sulfuric acid, fuming (H_2SO_4; Millipore Sigma, cat. no. 435597-500G)
  ▲ **CAUTION** H_2SO_4 is corrosive and can cause chemical burns. Wear gloves, a laboratory coat and eye protection when handling the material or its solutions. Dissolution of H_2SO_4 is highly exothermic, and the resulting heat may cause heat burns or ignite flammables.
- SYBR Green II dye (ThermoFisher Scientific, cat. no. S7564)
- *N*,*N*,*N*′,*N*′-tetramethylethylenediamine (TEMED), electrophoresis grade (Fisher, cat. no. BP150-20)
  ▲ **CAUTION** TEMED is a skin and respiratory tract irritant.
- Tert-butanol (Sigma, cat. no. 360538)
  ▲ **CAUTION** Tert-butanol is a highly flammable liquid and vapor, causes serious eye irritation, is harmful if inhaled and may cause respiratory irritation. Wear gloves and goggles.
- Triethylamine acetate, 2.0 M, pH 7 (TEAA; Glen Research, cat. no. 60-4110-60)
  ▲ **CAUTION** TEAA causes serious skin and eye irritation and may cause respiratory irritation. Wear gloves and goggles and dispense it in a vented hood.
- Triethylamine trihydrofluoride (Fisher Scientific, cat. no. AAL1441706)
- Tris base (Fisher, cat. no. BP-152-5)
- Tris[(1-benzyl-1H-1,2,3-triazol-4-yl)methyl]amine (TBTA; Sigma-Aldrich, cat. no. 678937)
- Triton X-100 (Sigma-Aldrich, cat. no. 93443)
- Trypsin-EDTA (1×) (Gibco by Life Technologies, cat. no. 15140-122)
- Universal support column, dimethoxytrityl (DMT) off (N-isopropyl [N-iPr]), 1,000 Å, 1 µmol, Luer (Bioautomation, cat. no. MLX1-3500-1)

- Urea, for molecular biology, DNase free, RNase free and protease free (Acros, cat. no. 327380050)
- Water (HPLC grade) (Fisher, cat. no. W5-4)
- Xylene cyanol (Sigma, cat. no. X-4126)
  ▲ **CAUTION** Xylene cyanol is a skin and respiratory tract irritant.

Equipment

- Agilent 1260 infinity HPLC system
- Amicon Ultra centrifugal filter, 10-kDa MWCO (Sigma, cat. no. UFC501008)
- Avance 300-MHz NMR I (Bruker)
- Biosafety cabinet (Thermo Scientific, model 1307)
- Biosset ASM-800 synthesizer
- Branson 1510 benchtop sonicator
- CombiFlash NextGen 300+ (Teledyne ISCO)
- Eppendorf centrifuge 5424 (Eppendorf)
- Flexible thin-layer chromatography (TLC) plates (Selecto Scientific, cat. no. 11078)
- Forma series II water jacket CO_2 incubator (Thermo Scientific)
- Freezer (−80 °C and −20 °C) and 4 °C refrigerator
- FV3000 confocal microscope (Olympus)
- Handheld Mineralight lamp (UVP, model UVGL-25)
- LSRII flow cytometer (Bioscience)
- Malvern Zetasizer
- Microfluor 1 96-well white microtiter plates (Thermo Scientific, cat. no. 14-245-194A)
- Milli-Q water-purification system
- NanoDrop 2000 spectrophotometer (Thermo Scientific)
- Olympus FV3000 confocal microscope (Olympus)
- pH meter (Fisher, dual channel pH/ion meter AR25)
- PCR machine (Eppendorf MasterCycler Gradient, model 5331)
- Real-time PCR detection system (Roche LightCycler 480 real-time PCR system)
- Polyacrylamide gel electrophoresis (PAGE) gel electrophoresis system (Hoefer, SE250 mighty small II for 8 × 7 cm gel)
- PLRP-S 4.6 × 250 mm 300 Å column (Agilent Technologies)
- Temperature-gradient gel electrophoresis (TGGE) system (Biometra, model 024-000)
- Optical microscope (Motic, cat. no. SFC-11)
- Savant DNA120 SpeedVac concentrator (Themo Electron)
- Synergy 4 microplate reader (Bio-Tek)
- Typhoon FLA 7000 imaging system (GE Healthcare)
- Waters Acquity ultra-performance liquid chromatograph and electrospray ionization-mass spectrometer (ESI-MS) with photodiode array and QDA detectors (Waters)
- Mfold (http://mfold.rna.albany.edu/?q=mfold/RNA-Folding-Form)
- FlowJo (https://www.flowjo.com/solutions/flowjo/downloads)
- ImageJ (http://rsbweb.nih.gov/ij/download.html); free download and installation. User instruction is also available online (http://rsbweb.nih.gov/ij/).
- MassLynx (https://www.waters.com/waters/en_US/MassLynx-Mass-Spectrometry-Software/nav.htm?locale=-&cid=513662)
- Mestrelab Nova (https://mestrelab.com/)

Reagent setup

▲ **CRITICAL** Prepare all reagents and perform all experiments by using pure water (Milli-Q, 18.2 MΩ cm^{-1} resistivity). Use DEPC-treated water for experiments involving RNA.
▲ **CAUTION** Wear gloves at all times.

Click solvent

This solvent consists of three parts DMSO and one part tert-butanol (3 ml of DMSO and 1 ml of tert-butanol). It should be freshly prepared to limit the solvent becoming wet.

CuBr stock solution
This solutions consists of freshly prepared 0.1 M CuBr in click solvent (1 mg of CuBr dissolved in 70 µl of click solvent).

TBTA stock solution
This solution is a 0.1 M solution of TBTA in click solvent (54 mg of TBTA dissolved in 1 ml of click solvent). It can be stored at −20 °C for 1 year.

Ascorbic acid stock solution
This solution is a 0.1 M solution of ascorbic acid in click solvent (10.0 mg of ascorbic acid dissolved in 570 µl of click solvent). It can be stored at −20 °C for 1 year.

Click solution
Add 1 volume of CuBr stock solution to 2 volumes of TBTA stock solution and 50 volumes of ascorbic acid to a final concentration of CuBr of 1.88 mM. The solution should be freshly mixed because of oxidation of Cu^{1+} to Cu^{2+}. Ascorbic acid will convert Cu^{2+} back to Cu^{1+} during the reaction.

0.05% (vol/vol) DEPC-treated water
Add 0.05 ml of DEPC to 99.5 ml of pure water and shake the solution vigorously. Incubate at 37 °C overnight and then autoclave the solution to remove DEPC. This reagent can be stored at room temperature (RT, 23 °C) for 1 year.

0.5 M EDTA, pH 8
Dissolve EDTA in pure water. Stir vigorously and adjust the pH to 8 with NaOH. This reagent can be stored at RT for 1 year.

TES buffer
This buffer consists of 50 mM Tris (pH 8.0), 50 mM NaCl and 1 mM EDTA. It can be stored at RT for 1 year.

Tris-borate EDTA (TBE) buffer, 1×
TBE buffer (1×) contains 89 mM Tris base, 200 mM boric acid and 2 mM EDTA. This buffer can be stored at RT for 1 year.

Tris-borate magnesium (TBM) buffer, 1×
TBM buffer (1×) contains 89 mM Tris base, 200 mM boric acid and 5 mM $MgCl_2$. This buffer can be stored at RT for 1 year.

3 M NaOAc, pH 6.5
Dissolve NaOAc in pure water. Adjust the pH to 6.5 with HAc. After autoclaving, this buffer can be stored at RT for 1 year.

2 M $MgCl_2$
This buffer can be stored at RT for 1 year.

Tris-EDTA saline (TES) buffer, 1×
TES buffer (1×) contains 50 mM Tris-HCl (pH 8.0), 100 mM NaCl and 2 mM $MgCl_2$. This buffer can be stored at RT for 1 year.

Urea denaturing PAGE gel, 10–15% (wt/vol)
Combine 10–15% (wt/vol; 37.5:1) acrylamide, 8 M urea, 10% (wt/vol) APS and TEMED. The gel should be freshly prepared and filtered to remove excess urea.

Native PAGE gel (TBM or TBE), 10–15% (wt/vol)
Combine 10–15% (wt/vol; 37.5:1) acrylamide, 1× Tris-borate buffer (pH 7.8), 10 mM $MgCl_2$ for TBM (or 2 mM EDTA for TBE), 10% (wt/vol) APS and TEMED. The gel should be freshly prepared.

RNA elution buffer, 1×
RNA elution buffer (1×) contains 0.5 M NH_4OAc, 10 mM EDTA and 0.1% (wt/vol) SDS in 0.05% (vol/vol) DEPC-treated water. After autoclaving, this buffer can be stored at RT for 6 months.

6× loading buffer
6× loading buffer contains 40% (wt/vol) sucrose, 0.1% (wt/vol) xylene cyanol superfine (FF) and 0.1% (wt/vol) bromophenol blue. This buffer can be stored at -20 °C for 1 year.

2× TBE loading buffer
2× TBE loading buffer contains 95% (vol/vol) formamide, 18 mM EDTA, 0.025% (wt/vol) SDS, 0.025% (wt/vol) bromophenol blue and 0.025% (wt/vol) xylene xyanol. This buffer can be stored at RT for 1 year.

10% (wt/vol) APS
10% (wt/vol) APS should be freshly made.

0.05 M phosphoramidite solution
Solid phosphoramidite (2′-tBDsilyl adenosine (n-bz) CED phosphoramidite, 2′-tBDsilyl cytidine (n-acetyl) CED phosphoramidite, 2′-tBDgilyl Guanosine (n-ibu) CED phosphoramidite, 2′-tBDsilyl uridine CED phosphoramidite, 2′-fluoro-2′-deoxy cytidine (n-ac) CED phosphoramidite, 2′-fluoro-2u-deoxy Uridine CED phosphoramidite, 2′-*O*-propargyl cytidine (n-bz) CED phosphoramidite, 2′-*O*-propargyl uridine CED phosphoramidite, 5′-hexynyl phosphoramidite or 5′-amino-modifier) is mixed with anhydrous ACN to reach a final concentration of 0.05 M for each phosphoramidite.
▲ **CRITICAL** The solution should be freshly prepared within an argon atmosphere to prevent water contamination.

1.5 M ammonium carbonate solution
Ammonium carbonate is mixed with water to reach a final concentration of 1.5 M. The solution can be stored at 4 °C in a sealed container for 1 year. Storage at RT may result in decomposition, thus affecting the solution's effectiveness.

0.1 M TEAA in water
100 ml of 2.0 M TEAA is mixed with water (HPLC grade) into a final volume of 2 liters. This solution can be stored at RT for 1 year.

0.1 M TEAA in 75% (vol/vol) ACN/water
100 ml of 2.0 M TEAA is mixed with 400 ml of water (HPLC grade) and then ACN (HPLC grade) is added and fixed at the final volume of 2 liters. This solution can be stored at RT for 1 year.

Equipment setup

Biosset ASM-800 synthesizer
The procedures listed in Box 1 outline the manufacturer's instructions for operating the oligo-synthesizer.

BOX 1

Operating the ASM-800 oligo synthesizer

▲ **CRITICAL** Phosphoramidite chemistry is highly sensitive to water, and water contamination greatly reduces reaction efficiency and therefore the yield of RNA synthesized. Ensure that all solutions and chemicals used on the oligo-synthesizer are dry and not in the presence of air or wet gas.

Open the synthesizer software

1. Launch the Oligo 800 synthesizer software on a computer connected to the ASM-800 oligo synthesizer equipment.

Pressurize the system

2. In the Oligo 800 software window, navigate to 'Auto Press' and click 'Start' to pressurize the system with argon gas. If the gas cylinder is changed, re-pressurize by using 'Auto Press'.

Manual mode activation

3. After pressurizing the synthesizer system, select 'Manual' in the Oligo 800 software menu to display a system diagram.

Column flushing with ACN

4. Flush the columns (W1a, W1b and W2) with ACN. In the 'Manual' window, select the columns, set the volume to 1,000 µl and the flow rate to 100 µl s^{-1} and initiate the flow. Repeat thrice to ensure that a total of 3 ml of ACN passes through the columns. During the flow, monitor the syringes for bubbles and air intake, ensuring that all bottles are sealed tightly.
5. If air is seen in the syringes, check and tighten each attached bottle and repeat the above procedures.

Inputting the RNA sequence to be synthesized

6. In the Oligo 800 software, click 'Sequence' and enter your sequence in capital letters or number according to the installed and desired phosphoramidite bottle from 5′ to 3′. For universal columns, input the entire sequence; if a specialty column is used, the first nucleotide may be included on the column. Save the inputted sequence by clicking the 'save' button.

Mounting the CPG support columns

7. Fit the CPG support columns tightly onto the instrument, ensuring that there are no gaps between the metal portion and the column frits.

Loading sequences and starting synthesis

8. In the Oligo 800 software, click 'Run' and delete any previous sequences by selecting the leftmost button on the first line and clicking 'delete all'. Load your sequences to the corresponding column locations.

Loading the synthesis program

9. In the 'Run' window, navigate to 'File' and select 'Open Program'. Delete any pre-loaded programs and select '200 nm RNA' for RNA synthesis.

Final deblocking protocol selection

10. Ensure that the 'Dpr' checkbox is checked to pause the synthesis at the final deblocking step to observe the final deblocking efficacy and guarantee the quality of synthesis strands.

Initiating and finishing the synthesis

11. Click the start button to begin synthesis. Upon completion, when the program pauses at the final deblocking step, select 'Continue' to finish the synthesis.

Drying the columns

12. In the 'Manual' window, select 'gas' and then the relevant column numbers, followed by 'waste'. Set the time to '100' and click 'start'. Repeat this thrice to dry the CPG thoroughly.

Removing the columns

13. Carefully disconnect the columns from the synthesizer, keeping the top connector on to avoid losing the column beads and RNA. Optionally, remove a blank column to release residual argon pressure. Place the support column in a 2-ml centrifuge tube.

Final steps

14. Reattach the blank column to the instrument and then transfer the CPG beads from the support column to the centrifuge tube by pushing them out.

Procedure

Synthesis of 4WJ component strand oligos

● **TIMING** ~1 week

▲ **CRITICAL** Phosphoramidite chemistry is highly sensitive to water, and water contamination greatly reduces reaction efficiency and therefore the yield of RNA synthesized. Ensure that all solutions and chemicals used on the oligo-synthesizer are dry and not in the presence of wet air or gas.

1. Set up the Biosset ASM-800 synthesizer by following the manufacturer's procedures and the instructions in Box 1. Prepare the synthesizer column onto the oligosynthesizer by attaching the universal support column to the synthesizer. Once it is attached, flush the column with ACN three times by following the instructions in Box 1.
2. Input the sequences for $4WJ_A$-6 Alk, $4WJ_B$-6 Alk, $4WJ_C$-6 Alk-EGFR, $4WJ_D$-6 Alk or $4WJ_D$-5′ Amine found in Table 1 or the desired nanoparticle sequence. The synthesizer can handle up to eight different sequences simultaneously because of its eight column locations and channels; therefore, each strand can be synthesized at once.
3. Initiate RNA synthesis by clicking 'Start' to begin the loaded protocol with the following steps. These steps are automated by the synthesizer and do not require user input.
   (i) Addition step. Add both the acidic catalyst 5-ethylthio-1H-tetrazole and phosphoramidite to the controlled pore glass (CPG) column. Use a molar ratio of CPG seed to phosphoramidite of 1:20 and a ratio of phosphoramidite to 5-ethylthio-1H-tetrazole of 1:5. Follow the coupling time recommended by the phosphoramidite provider.
   (ii) Oxidation step. After addition, wash the CPG column with ACN three times. Then, add 200 µl of oxidizer to the column and let it react for 2 min.
   (iii) Capping step. After oxidation, wash the CPG column with ACN three times. Add equal amounts of capping reagent A and capping reagent B, totaling 200 µl each, and allow the reaction to proceed for 2 min.
   (iv) Deprotection step. After the capping step, wash the CPG column with ACN three times and then with dicholoromethane (DCM) once. Add 600 µl of 3% (vol/vol) TCA in DCM as the deprotecting reagent, allowing it to react for 1 min.
   (v) Repeat steps. Repeat the capping and deprotection steps until the final base is added and deprotected.
4. After synthesis completion and the final deprotection step, dry the columns by using argon gas from the instrument. In the Oligo 800 software, go to the 'Manual' window, select 'gas', choose the column numbers and then 'waste'. Set the time to '100' and click 'Start'. Repeat three times to ensure complete drying.
   ■ **PAUSE POINT** RNA oligo synthesis can be paused before final deprotection and synthesis. Columns can be stored at −20 °C until further use in the short term (6 months).
5. Remove the column from the synthesizer and transfer the CPG beads into a 2-ml centrifuge tube by following the instructions in Box 1.
6. Add 1.5 ml of a 1:1 solution of ammonium hydroxide and methylamine to the centrifuge tube containing the CPG beads to cleave synthesized RNA from the beads and carry out final base deprotection of base-protecting groups of the RNA. Incubate at room temperature for 2 h. Use the provided metal tube holder to manage the pressure and keep the tube lids closed. After incubation, cool the tubes on ice for 10 min before opening them in a chemical fume hood to release any pressure.
7. Centrifuge the RNA-containing tubes by using a benchtop mini-centrifuge at 2,000*g* for 30 s to spin down the CPG beads; then, decant the supernatant containing RNA into a new 1.5-ml centrifuge tube.
   ■ **PAUSE POINT** RNA oligo processing can be paused before drying, and the solution can be stored at −20 °C until further use in the short term (6 months).
8. Dry the mixture to remove all solvent by using a speed vacuum concentrator overnight.
9. After drying, resuspend the RNA in 250 µl of DMSO. Heat to 65 °C for ~5 min if necessary to fully dissolve the RNA.
10. Add 250 µl of triethylamine trihydrofluoride (TEA·3HF) to the RNA/DMSO mixture and incubate at 65 °C for 2.5 h by using a metal tube holder to deprotect the 2′ location of the RNA ribose. Manage the pressure buildup during heating. After incubation, cool the tubes on ice for 10 min. Finally, transfer the solution into a new 15-ml centrifuge tube.
    ▲ **CRITICAL STEP** Wear gloves when handling TEA·3HF.
11. To neutralize the solution, quench the acid (TEA·3HF) with 1.5 ml of 1.5 M ammonium carbonate. Add the ammonium carbonate slowly and with caution to manage the bubbling reaction.

Table 1 | Sequences of RNA nanoparticles

RNA strand	Sequence (5′–3′)
$4WJ_A$	5′-uuAGGuAAAGccAccuGcAGGuGcuAccGAuGu AAuucAA-3′
$4WJ_B$	5′-uuGAAuuAcAucGGuAGcAcGGGcuGuGcGAG GcuGAAcAG-3′
$4WJ_C$-$EGFR_{apt}$	5′-cuGuucAGccucGcAcAGccAGcAcGcAccuGAA uAGGuGccuuAGuAAcGuGcuuuGAuGucGAuucG AcAGGAGGc-3′
$4WJ_C$	5′-cuGuucAGccucGcAcAGccAGcAcGcAccuGAA uAGG-3′
$4WJ_D$	5′-ccuAuucAGGuGcGuGcuGGGcuGcAGGuGGc uuuAccuAA-3′
$4WJ_A$-6-ALK	<u>5′</u>-uuAGGuAAAGccAccuGcAGGuGcuAccGAuGu AAuucAA-3′
$4WJ_B$-6-ALK	<u>5′</u>-uuGAA<u>u</u>uAcA<u>u</u>cGGuAGcAcGGGcuGuG<u>c</u>GAG G<u>c</u>uGAA<u>c</u>AG-3′
$4WJ_C$-6-ALK-$EGFR_{apt}$	<u>5′</u>-cuGuu<u>c</u>AGcc<u>u</u>cGcAcAGccAGcA<u>c</u>GcAc<u>c</u>uGAA <u>u</u>AGGuGccuuAGuAAcGuGcuuuGAuGucGAuucGAcAGG AGGc-3′
$4WJ_C$-6-ALK	<u>5′</u>-cuGuu<u>c</u>AGcc<u>u</u>cGcAcAGccAGcA<u>c</u>GcAc<u>c</u>uGAA <u>u</u>AGG-3′
$4WJ_D$-6-ALK	<u>5′</u>-ccuAu<u>u</u>cAGG<u>u</u>GcGuGcuGGGcuGcAGG<u>u</u>GGc u<u>u</u>uAcc<u>u</u>AA-3′

All C and U are 2′-fluoro modified (lowercase). All 5′ are 5′-hexynyl modified, and all underlined C and U are 2′-O-propargyl modified.

12. To desalt and remove early aborted strands, prepare the Glen Gel-Pak 2.5 desalting column by flushing it with 50 ml of water. Load RNA solution from the centrifuge tube onto the Glen Gel-Pak 2.5 desalting column. Allow ~2 ml of liquid to pass through, then add 1 ml of water at a time and collect five fractions. Fractions 2–4 are expected to contain the desalted RNA.
13. Combine the fractions for further usage and verify RNA concentrations by using a NanoDrop spectrophotometer or similar UV spectrophotometer. RNA oligos can be stored at −20 °C for short-term (6 month) storage or at −80 °C for long-term (>1 year) storage.
◆ **TROUBLESHOOTING**

Chemical synthesis of a chemotherapeutic prodrug

● **TIMING** ~1 week

14. Add 0.234 mmol (1 equiv.) of 6-azidohexanoic acid, 0.046 mmol (0.2 equiv.) of 4-dimethylaminopyridine and 0.468 mmol (2.0 equiv.) of chemotherapeutic (PTX, SN-38 or CPT) into a dry round-bottom flask filled with inert atmosphere gas (i.e., nitrogen or argon gas). Dissolve in 4 ml of anhydrous dichloromethane and mix constantly with a stir bar for 5 min at 0 °C (in an ice bath).
▲ **CRITICAL STEP** Esterification of the chemical drugs requires a dry environment. The presence of water or humidity could critically affect the yield of the prodrug.
15. In another dry round-bottom flask filled with inert atmosphere gas (i.e., nitrogen or argon gas), add 0.234 mmol (1 equiv.) of *N*,*N*′-dicyclohexylcarbodiimide (DCC) dissolved in 1 ml of anhydrous dichloromethane and stir the reaction for 10 min or until all DCC dissolves.
16. Add the DCC solution (Step 15) to the reaction mixture (Step 14) dropwise for 5 min and continue stirring the reaction for ≥12 h in an ice bath under a nitrogen or argon gas environment.
■ **PAUSE POINT** If DCC is used as a coupling agent, a white precipitate will appear because of the formation of an insoluble acyl urea by-product. EDC does not form such a precipitate because its urea by-product is generally soluble in dichloromethane.
17. Check whether Steglich esterification of the chemotherapeutic into the prodrug took place by completing TLC on chemotherapeutic-azide to the reaction mixture as follows:
    (i) Deposit 5 drops of each sample 1 cm from the bottom of the TLC plate by using capillary glass tubing and adding one drop at a time, allowing each drop to dry before adding an additional drop.
    (ii) Place 1 ml of TLC solvent (50% n-hexane/50% ethyl acetate (vol/vol)) into the bottom of a chromatography glass chamber and cover it with the lid to minimize the evaporation of the volatile solvent.
    (iii) Insert the TLC plate into the chromatography glass chamber and cover it with the lid, making sure that sample spots are not submerged in the TLC solvent.

(iv) Allow the solvent to run up the TLC plate until reaching ~5 mm from the top of the TLC plate.

(v) Remove the TLC plate from the chamber, allow it to air dry and image UV shadow to check compound migrations by using a UV lamp.

▲ **CAUTION** TLC should be completed in a vented hood to prevent exposure to hazardous chemicals.

▲ **CRITICAL STEP** Additional staining with 5% sulfuric acid in 95% ethanol (vol/vol) may be needed to confirm the synthesis of the prodrug and detect any impurities that may appear during the reaction, to ensure the purity of the prodrug. To perform the staining, spray the TLC plate with 5% sulfuric acid in 95% ethanol (vol/vol) and dry it in the oven for 5–10 min.

▲ **CRITICAL STEP** The retention factor (Rf) value of both the substrate drug and the prodrug can be calculated during the TLC plate experiment for quality control purposes. The Rf value is calculated as Rf = distance traveled by solute/distance traveled by solvent. Distance should be measured and quantified between defined start and end lines (1 cm from the bottom of the plate and 5 mm from the top of the plate, respectively). When the solvent reaches the end line, pull the plate out and measure the Rf of both the substrate drug and the prodrug. An Rf number for either the substrate drug or the prodrug between 0.7 and 0.3 is considered acceptable. The Rf value difference between the substrate and prodrug is expected to be larger than 0.2, with the prodrug (chemotherapeutic-azide) having a larger Rf value over chemotherapeutics and all reactants.

18. Upon confirmation of reaction completion, concentrate the reaction by evaporating on a rotary evaporator. Then, redissolve the dried prodrug in 10 ml of ethyl acetate to form a white precipitant of dicyclohexylurea (DCU). Filter DCU precipitant with filter paper and wash the organic fraction with saturated sodium bicarbonate solution and brine.

▲ **CRITICAL STEP** Filtering is not necessary if using EDC as a coupling agent.

◆ **TROUBLESHOOTING**

19. Dry the organic fraction over anhydrous sodium sulfate to absorb the water or moisture. Filter through filter paper and concentrate by using a rotary evaporator.

20. The purification of the prodrug from a chemotherapeutic and azide linker is critical for ensuring the click chemistry reaction with RNA and full removal of DCU. Purify chemotherapeutic prodrugs from reactants and by-products via CombiFlash (Teledyne Labs) (option A) or silica (SiO_2) column chromatography (option B) as follows:

(A) **CombiFlash (Teledyne Labs)**

(i) Follow the equipment setup in Box 2.

(ii) Load 100 mg of chemical into the CombiFlash silica column and air-dry the column.

(iii) Use *n*-hexane (solvent A) and ethyl acetate (solvent B) at different specific ratios to wash off the product from the CombiFlash silica column, starting the wash with 100% solvent A for 3 min.

(iv) Gradually change the ratio of solvents from 100% solvent A/0% solvent B (vol/vol) to 13% solvent A/87% solvent B (vol/vol) over 10 min. The prodrug will elute off the column through the solvent gradient (i.e., SN38-N_3 washes off at 13% solvent A/87% solvent B during the 5-min plateau wash).

(v) Purified prodrug is automatically collected and re-concentrated by removing the solvent. Also collect the remaining samples that are eluted out at 80% DCM/20% methanol (vol/vol) during the cleanup and shutdown procedures of the CombiFlash in Box 2 to ensure that samples are in the collected product and not discarded here.

(B) **Silica (SiO_2) column chromatography**

(i) In a glass column with a stopcock on the lower end fitted with glass wool, close the stopcock and fill the column with dry silica gel.

(ii) Slowly fill 3/4 of the column with solvent (90% *n*-hexane/10% ethyl acetate (vol/vol)). Open the stopcock and let the solvent pass through the silica gel. Pack the silica gel by applying pressure gas from the top of the column while the solvent

BOX 2

Operating the CombiFlash NextGen 300+

Solvent attachment

1. Degas a 500-ml bottle of each of the following HPLC-grade solvents by using a Branson 1510 benchtop sonicator for 30 min. Attach each solvent to the corresponding CombiFlash NextGen 300+ tubing connected by following the manufacturer's instructions.
   Solvent A: *n*-hexane
   Solvent B: ethyl acetate
   Solvent C: dichloromethane
   Solvent D: methanol

Software initialization

2. Open the embedded software within CombiFlash NextGen 300+. Click on 'Reset'.

Mobile phase prime

3. Click on 'Tools' and then 'Autoprime'.
4. Prime with ethyl acetate first and then *n*-hexane.
5. Click 'Play' to prime the system.

Setting up the column and system

6. Pour dried silica gel provided with the sample into a solid loading cartridge, put a frit onto the top and pack the cartridge according to the manufacturer's suggestions.
   ▲ **CAUTION** This step should be completed in a chemical fume hood to avoid inhalation of silica gel.
7. Place solid loading cartridge onto the CombiFlash and connect the pipeline with the cartridge according to the manufacturer's suggestions.
8. Place the silica gel disposable flash columns onto the CombiFlash. Choose the column type according to the manufacturer's suggestions.
9. In the software, go to 'Tools' → 'Manual Control' → 'Flow Path' → 'Through Column and Flow Cell'. Prime the system with solvent A.
10. Place the tube rack with empty tubes into the CombiFlash.

Program setup

11. In the software, go to the method editor.
12. Set up the suggested flow rate and equilibrium volume according to the recommendation on the silica gel column.
13. Collect all fractions by clicking 'Peak Collection' → 'All'.
14. Select 254 nm, 280 nm and all wavelength in the 'Peak Detection Section'.
15. Set the running protocol according to the compounds. For SN38-N_3, the product will wash off at 13% hexane and 87% ethyl acetate (vol/vol).
   ▲ **CRITICAL STEP** Equilibrate the column by using 100% *n*-hexane. Avoid using a high percentage of ethyl acetate during equilibration, because it may cause cracking of the silica column. Gradually increase the ethyl acetate fraction during the elution process.
16. Save the changes and go back to the main menu in the software.

Run and finish

17. In the software, select 'Start' on the main menu.
18. Select the start rack and start tube.
19. Select 'Solid' under the sample loading option.
20. Disconnect the cartridge and column from the system after finishing.

passes through. Repeat the process several times until the silica gel is packed, drain excess solvent until just above the silica stationary phase and close the stopcock.

(iii) Add silica gel to a round-bottom flask containing a concentrated solution of the mixture of prodrug until a slurry is formed (add 2–4 ml of ethyl acetate if necessary). Concentrate by using a rotary evaporator until dry.

(iv) Add the dry silica gel containing the prodrug to the column containing packed silica gel and cover it with glass wool.

(v) Elute samples by using the same solvent system used in TLC (90% *n*-hexane/10% ethyl acetate (vol/vol) to 50% *n*-hexane/50% ethyl acetate (vol/vol)), ensuring that by-products elute off the column followed by product. Collect and fractionate the elution and test for which fraction has prodrug product via TLC as in Step 17.

21. Combine all fractions with the product and concentrate by using a rotary evaporator. The chemotherapeutic prodrug is now considered pure and ready for conjugation to an RNA oligo.
   ■ **PAUSE POINT** The chemical prodrug can be stored at −20 °C until further use for 1 year.
22. Verify chemotherapeutic prodrug formation by both NMR (option A) and mass spectrometry (option B), demonstrating the presence of ester formation and the presence of 1-azidohexane linker (option A) and corresponding mass increase (option B), respectively (Fig. 7).
   (A) **NMR of the chemotherapeutic prodrug (Fig. 7a)**
      (i) Dissolve 2–4 mg of the prodrug in 0.5 ml of an appropriate deuterated solvent (i.e., deuterated chloroform, $CDCl_3$).

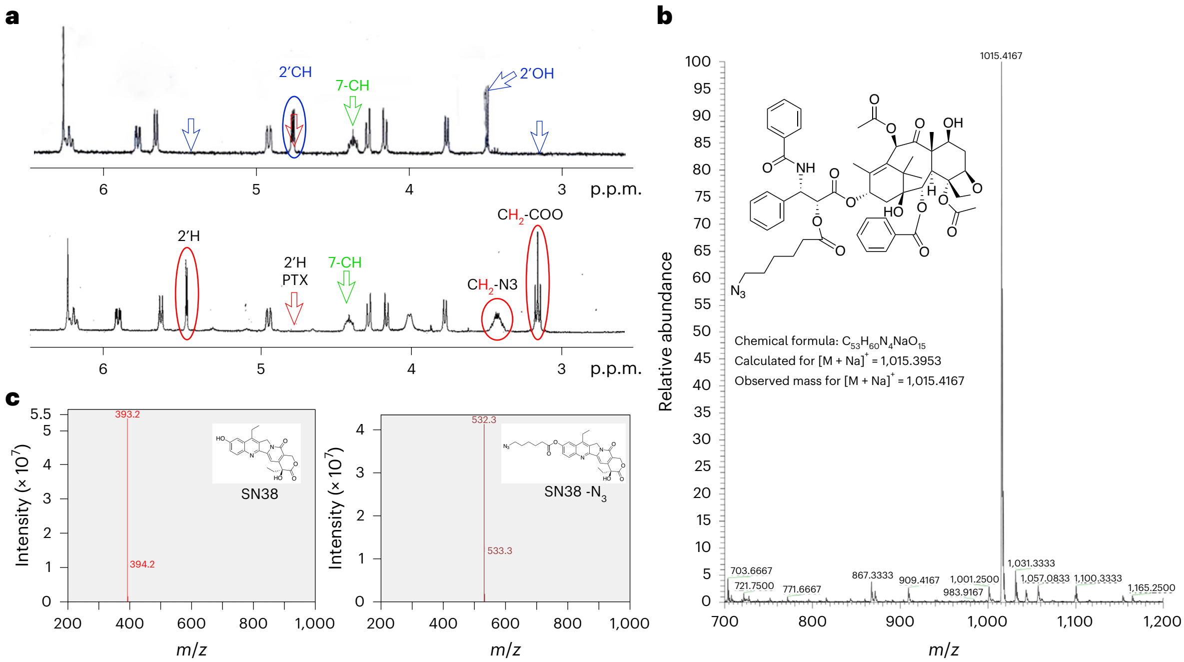

Fig. 7 | Characterization of prodrugs after Steglich esterification. a, ^{1}H NMR (400 MHz) for PTX. Circles and arrows show identifying groups to demonstrate successful conversion of PTX (top) into PTX-azide (bottom). **b**, Mass spectra of PTX-azide: ESI-MS calculated for $C_{53}H_{60}N_4NaO_{15}$ is 1,015.3953, and the observed mass is 1,015.4167. **c**, Liquid chromatography-mass spectrometry data of the synthesized SN38-N_3. Panel **a** reproduced with permission from ref. 64, Elsevier. Panel **b** adapted with permission from ref. 34, Elsevier. Panel **c** adapted with permission from ref. 43, Elsevier.

(ii) Transfer the prodrug solution into the dry NMR tube and cap the NMR tube to prevent evaporation.
(iii) Launch the Bruken Topspin 2.1 program. Type 'edc' into the command line on the bottom left of the software interface to create a new experiment and choose the appropriate NMR experiment (i.e., proton, carbon, etc.) in the instrument.
(iv) Place the NMR tube into the spinner and adjust it to the correct sample height. Use the depth gauge in the spinner to set the correct depth.
(v) Type 'ej' into the command line to create airflow in the sample loader. Place the sample in the NMR instrument and type 'ij' (inject sample) to lower the NMR tube containing the sample into the magnetic field.
(vi) Type 'lock' to lock the solvent signal of the sample.
▲**CRITICAL STEP** The solvent signal must match the solvent used to dissolve the prodrug, as above. Failure to lock the correct solvent or using the wrong solvent will result in a shift of the signal to an incorrect p.p.m.
(vii) Perform necessary tuning by typing 'atma', followed by shimming by typing 'topshim' to optimize the magnetic field and produce a good spectrum.
(viii) Retrieve the solvent information by typing 'getprosol'.
(ix) Set the number of the scans by typing 'ns' and adjust the scan as necessary.
(x) Begin data acquisition by typing 'rga' and 'zg'.
(xi) Once the experiment is finished, type 'efp' and 'apk' to process NMR data.
(xii) Type 'ej' to retrieve the sample.
(xiii) Gently lift the NMR tube and spinner from the loader.
(xiv) Stop the airflow from the loader by typing 'ej'.
(xv) Further analyze NMR data in Mestrelab Nova or other NMR software by following the manufacturer's guidelines.
◆**TROUBLESHOOTING**

(B) **Mass spectrometry of the chemotherapeutic prodrug (Fig. 7b,c)**

(i) Prepare the prodrug sample for mass spectrometry by dissolving 100 µg of the prodrug in 1 ml of a 50:50 (vol:vol) mixture of methanol and water. Place the sample into an HPLC glass vial. Also prepare control samples (a blank sample consisting of solvent only and the native chemotherapeutic drug dissolved in the same solvent).

(ii) Launch MassLynx software and then select 'shortcut, instrument' and then 'inlet method'.

(iii) Launch OA Manager from the MassLynx window by choosing 'shortcut', then 'openlynx' and then 'OA Manager'.

(iv) Launch OA Login from the shortcut on the desktop.

(v) Prime the pump by selecting 'ACQUITY additional status' and then right-click in the section 'Binary Solvent Manager'.

(vi) Select 'Prime A/B solvent' and then wait for 2 min.

(vii) Submit the samples by opening the OA Login window and clicking 'sample'. Follow the instructions provided by the wizard.

(viii) Pick methods and load samples to the Waters Acquity ultra-performance liquid chromatograph and ESI-MS by following the manufacturer's guidelines. Run the samples.

Conjugation of prodrug-azide to 4WJ component strand via click chemistry

● **TIMING** 4–5 d

23. Dissolve the prodrug in click solvent to ensure solubilization of poorly aqueous soluble drugs. Ensure that the reaction does not become turbid, with a minimum ratio of 50% water and 50% organic solvent (vol/vol).
▲ **CRITICAL STEP** If the reaction becomes turbid or a precipitant is seen, add more click solvent to the reaction.
24. For incorporation of prodrug-azide into alkyne-modified RNA, a ratio of 5 prodrugs to 1 alkyne modification is generally desired. That means a ratio of 30 prodrugs to 1 RNA is required. Add the desired amount of RNA to the dissolved prodrug for each 4WJ component strand reaction ($4WJ_A$, $4WJ_B$, $4WJ_C$ and $4WJ_D$).
▲ **CRITICAL STEP** The ratio of prodrug to RNA/alkyne modification can be varied and titrated across multiple ratios to test the best conjugation methodology.
25. Add click solution (composed of CuBr, TBTA and ascorbic acid) to the reaction at a ratio of 1:20 of alkyne modification to CuBr and vortex the reaction for 30 s.
▲ **CRITICAL STEP** Copper II (Cu^{2+}) is required to catalyze this reaction but increases reactive oxygen species and free radicals that can be quite damaging to biological samples, including RNA. Cu^{2+} ions can promote the backbone cleavage of RNA strands or permanent base modification[212,213]. It is critical that the time of incubation of Cu^{2+} with RNA is controlled, free Cu^{2+} is removed after the click reaction (see Step 30) and the quality of the RNA strands is confirmed by gel electrophoresis as described in Step 31.
26. Incubate the reaction at RT overnight.
▲ **CRITICAL STEP** If the reaction is not completed or turbidity is seen, the reaction can be heated to 37 °C. Heating the reaction over a prolonged time period may promote RNA degradation.
■ **PAUSE POINT** Click reaction of the chemical drug and RNA oligo can be paused and stored at −20 °C for ≤6 months.
27. Ethanol-precipitate RNA products from the click chemistry reaction to remove click solvent and excess copper catalyst by adding 2.5 volumes of 100% ethanol and 0.1 volume of 3 M sodium acetate. Allow precipitation to occur overnight at −20 °C.
28. Centrifuge the mixture at 16,500*g* for 30 min at 4 °C and remove the supernatant; wash the pellet with 70% (vol/vol) ethanol and dry the pellet for 5 min with a SpeedVac concentrator.
29. Rehydrate the pellet in DEPC-treated water.
■ **PAUSE POINT** The click reaction of the chemical drug and RNA oligo can be paused and stored at −20 °C for ≤6 months.
◆ **TROUBLESHOOTING**

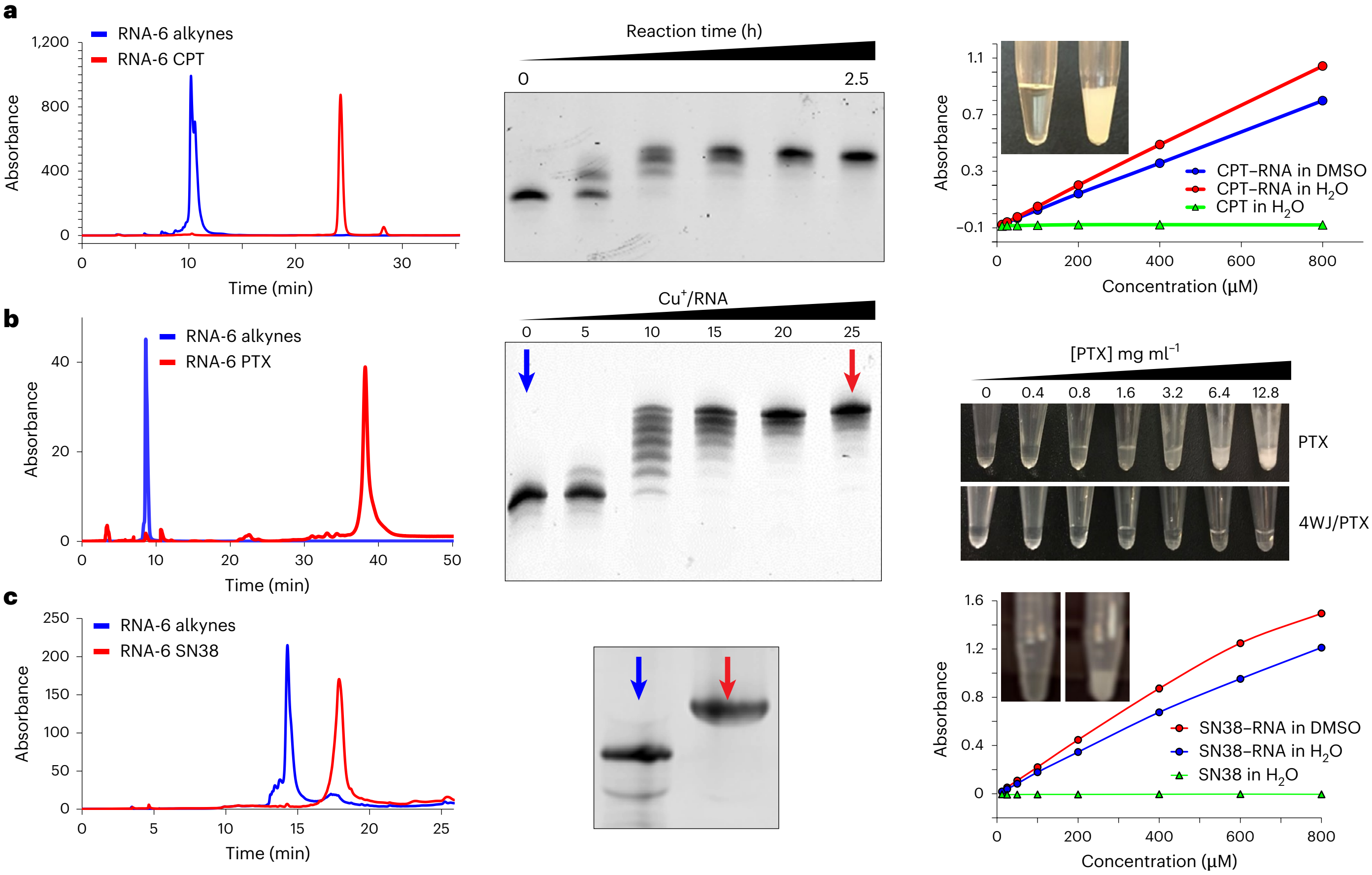

Fig. 8 | Characterization of RNA oligos conjugated with chemotherapeutics. RNA conjugates analyzed by reverse-phase HPLC (left), 15% (wt/vol) urea denaturing PAGE in TBE (middle) and chemical drug solubility measured by absorbance at 354 nm (CPT) and 366 nm (SN38) (right) for CPT (**a**), PTX (**b**) and SN38 (**c**). Panel **a** adapted from ref. 42, CC BY 4.0 (https://creativecommons.org/licenses/by/4.0/). Panel **b** adapted from ref. 41, CC BY 4.0 (https://creativecommons.org/licenses/by/4.0/). Panel **c** adapted with permission from ref. 43, Elsevier.

30. Purify 4WJ component strands conjugated with a prodrug (from Step 29) to remove the non-reacted prodrug, unlabeled oligos and copper catalyst by using either a 15% (wt/vol) 8 M urea denaturing PAGE gel run in TBE buffer (option A) or reverse-phase HPLC (Fig. 8, left panel) (option B).
   (A) **Denaturing PAGE gel purification**
      (i) Add RNA to an equal volume of 2× denaturing loading dye and load samples into the wells of a 15% (wt/vol) 8 M urea denaturing PAGE gel. Run the gel at 120 V for ~100 min.
      (ii) Excise the band corresponding to the conjugated 4WJ component strand under UV light (254 nm), cutting the band into small (~2 × 2 mm) pieces. Elute the RNA by using RNA elution buffer by completely submerging the gel pieces in buffer in a microcentrifuge tube at 37 °C for 4 h.
      (iii) Pipette off and keep the supernatant from the elution step, leaving behind the gel pieces in the tube, and add to it to 2.5 volumes of 100% ethanol and 0.1 volume of 3 M sodium acetate. Allow precipitation to occur overnight at −20 °C.
      (iv) Centrifuge the mixture at 16,500*g* for 30 min at 4 °C and remove the supernatant; wash the pellet with 70% (vol/vol) ethanol and dry the pellet for 5 min with a SpeedVac concentrator.
      (v) Rehydrate the pellet in DEPC-treated water of the desired volume.

BOX 3

Operating the Agilent 1260 Infinity Quaternary liquid chromatograph

Startup procedure

Column installation

1. Connect the PLRP-S 4.6 × 250 mm 300-Å column to the HPLC system by following the manufacturer's instructions.

Solvent attachment

2. Degas a 1-liter bottle of each of the following solvents by using a Branson 1510 benchtop sonicator for 30 min. Attach the following buffers to the corresponding tubing connected to the HPLC pump by following the manufacturer's instructions.
   Solvent A: 0.1 M TEAAs in HPLC water
   Solvent B: 0.1 M TEAAs in 75% (vol/vol) HPLC ACN
   Solvent C: 100% HPLC grade ACN
   Solvent D: 100% HPLC grade water

Software initialization

3. Open the OpenLab (online) software.

Method creation

4. Select 'New method from the instrument' to enter the software interface.

Mobile phase composition

5. Right-click on the 'Quat. Pump' block and select 'Method'.
6. Adjust the solvents to 95% C and 5% D (vol/vol) in the pop-up window.
7. Click 'Apply' to execute the change.

Column temperature adjustment

8. Right-click on the 'Column Comp.' block.
9. Input the desired temperature for both left and right sides.

Signal acquisition

10. Set up signal acquisition at 260 nm in the 'MWD' module for maximal UV absorption of RNA.

Initial run

11. Click the green 'On' button to start the run with 95% solvent C and 5% solvent D (vol/vol) at a flow rate of 1.0 ml min^{-1} for 30 min to allow for equalization of the column.

Mobile phase change

12. Change the mobile phase to 50% solvent A and 50% solvent B (vol/vol) at 1.0 ml min^{-1} for 5 min.

Column conditioning

13. Condition the column with 95% solvent A and 5% solvent B (vol/vol) at 1.0 ml min^{-1} for 30 min.
14. The system is now conditioned and ready for RNA loading for purification.

Shutdown procedure

Column washing

1. Wash the column with 95% solvent C and 5% solvent D (vol/vol) at 1.0 ml min^{-1} for ≥30 min.
2. Heat the column to 80 °C during washing.

Baseline signal

3. Continue washing until the UV absorbance signal in the online plot reaches baseline.

Temperature adjustment and flushing

4. Reduce the column temperature to 25 °C.
5. Flush the column by using 50% solvent C and 50% solvent D (vol/vol).
   ▲ **CRITICAL STEP** Ensure that the mobile phase contains ≥1% solvent C and never use 100% solvent D (vol/vol).

System shutdown

6. Power off the high-performance liquid chromatograph by clicking the red 'Off' button in the software.

(B) **Reverse-phase HPLC purification**

(i) Follow the HPLC equipment setup procedure (Box 3) to set up the system and prepare for RNA loading and purification.

(ii) After conditioning of the column, set the signal baseline to zero in the 'Online Plot' tab of the software by clicking the 'Balance' button.

(iii) Load an RNA-purifying method in the HPLC software by clicking the 'Method' tab on the top bar and select the desired method for RNA purification. The parameters for the methodology should be as follows. The first 10 min will be a constant wash with a mixture of 95% A and 5% B (vol/vol) at a 1 ml min^{-1} flow rate. A continuous change of mixture from 95% A and 5% B to 5% A and 95% B (vol/vol) will be set during the next 60 min at 1 ml min^{-1}. The final 10 min will be a constant wash with a mixture of 5% A and 95% B (vol/vol) at 1 ml min^{-1}.

(iv) Input the sample information into the HPLC software by clicking 'RunControl' and select 'Sample Info' to input sample information and specify the saving folder.

(v) To initiate the loading of RNA sample into the injection loop, set the injector to 'LOAD' and load 500 µl of 100% ACN into the injector three times.

Continue washing the loop with 500 µl of HPLC-grade water three times to flush out the ACN.

▲ **CAUTION** Always flush with water after ACN to prevent ACN residue from interfering with sample interaction with the column.

(vi) Click the 'Method' tab on the software and select 'Save Method' before running. Ensure that any changes to the method are saved before proceeding.

(vii) Set up the fraction collector by resetting the fraction collector to its initial position. Right-click on the fraction collector module and select 'Reset Fraction Collector'. Turn on collection by selecting the method and changing the setting from 'off' to 'Time-based with timeslices' (0.5 min or 1 min) or 'Peak-based' collection. Choose 'Assign Wellplates' to assign the blocks for 96-well plates. Set up clean 96-well collection plates in the fraction collector blocks.

(viii) Inject and load the RNA sample into the injector by using a clean glass syringe. Flip the injector valve to the 'INJECTION' position to automatically start the run. The drug-labeled RNA will be separated from unreacted RNA-6 alkynes by using a 95% water and TEAA/5% ACN and TEAA to 5% water and TEAA/95% ACN and TEAA (vol/vol) gradient controlled by the method selected in the software. The unreacted RNA-6 alkynes will be collected at around 70% water and TEAA/30% ACN and TEAA (vol/vol), and the conjugated RNA-6 drugs will be collected at around 20% water and TEAA/80% ACN and TEAA (vol/vol). Samples will be automatically collected, and fractions are collected on the basis of the wash-off time.

(ix) At the completion of the run, move the injector back to the 'LOAD' position. Collect fractions from the fraction collector for analysis. Shut down the high-performance liquid chromatograph by following the manufacturer's recommended procedure and shutdown procedure in Equipment setup.

(x) Analyze the 260-nm absorbance of fractions under the 'Data Analysis' tab of the software. Select the peaks of interest and keep the corresponding fraction numbers for further processing.

▲ **CAUTION** If there are multiple peaks of purified RNA on the 260-nm absorbance and uncertainty in which peak corresponds to the drug-conjugated 4WJ strand, save all peaks and perform further gel analysis (as in Step 30A(i) above without excising bands) to determine the actual peak of interest. Image gel stained with ethidium bromide on a gel imager such as a Typhoon FLA 7000 (GE Healthcare).

▲ **CRITICAL STEP** Ethidium bromide is toxic, and an alternative fluorescent nucleic acids dye can be used as a safe alternative. SYBR Green II dye is specifically designed for RNA intercalation and can be used to stain gels.

(xi) Dry the collected fractions by using a SpeedVac concentrator overnight. Once the samples are dried, resuspend the fractions containing RNA products with DEPC-treated water. Concentrate the RNA by loading 500 µl of the RNA product into an Amicon Ultra centrifugal filter with a 10-kDa MWCO and a 0.5-ml sample volume. Spin at 14,000*g* for 15 min and collect the fraction from the filter device sample reservoir. RNA is now purified and ready for future steps.

31. Confirm chemical drug conjugation to the 4WJ oligo strand by running a 15% (wt/vol) urea denaturing PAGE gel in TBE buffer (Fig. 8, middle panel).

(i) Mix ~250 ng of RNA conjugated with the chemical drug (including RNA with no drug controls) with an equal volume of 2× running buffer to generate samples to be loaded into the gel.

(ii) Prepare and run 15% (wt/vol) urea denaturing PAGE in TBE buffer of RNA samples at 150 V for 1 h.

(iii) Stain the gel in ethidium bromide (or an alternative, as above) containing TBE buffer and visualize on a gel imager (e.g., Typhoon FLA 7000 (GE Healthcare)).

◆ **TROUBLESHOOTING**

■ **PAUSE POINT** RNA oligos can be stored at −20 °C for ≤6 months or at −80 °C for long-term (>1 year) storage.

Assembly of ultra-stable 4WJ RNA nanoparticles harboring chemotherapeutics

● **TIMING** 2–3 d

32. The 4WJ RNA nanoparticle assembles into an ultra-stable complex consisting of the four component strands. Combine $4WJ_A$, $4WJ_B$, $4WJ_C$ and $4WJ_D$ strands at an equimolar ratio in TES buffer. Then, denature RNA strands at 95 °C for 5 min, followed by gradual cooling to 4 °C over the course of 1 h in a thermal cycler.
33. Assay the assembly of the 4WJ nanoparticle by using a 12% (wt/vol) native PAGE gel run in TBE buffer at 120 V for 1 h and compare its migration to single strands and partial 4WJ assemblies. Stain the gel in ethidium bromide (or an alternative, as above) containing TBE buffer and visualize on a gel imager (e.g., Typhoon FLA 7000 (GE Healthcare)) (Fig. 9a).
34. Purify the 4WJ assemblies by 12% (wt/vol) native PAGE gel run in TBE buffer at 150 V for 1 h. Excise the band corresponding to the assembled 4WJ construct under UV light (254 nm). Elute the RNA by using RNA elution buffer containing 10 mM Mg^{2+} at 37 °C for 4 h, as in Step 30(A)ii.
35. Take the supernatant from the elution step and add it to 2.5 volumes of 100% ethanol and add 0.1 volume of 3 M sodium acetate. Allow precipitation to occur overnight at −20 °C.
36. Centrifuge the mixture at 16,500*g* for 30 min at 4 °C and remove the supernatant; wash the pellet with 70% (vol/vol) ethanol and dry the pellet for 5 min with a SpeedVac concentrator.
37. Rehydrate the pellet in TES buffer of the desired volume (normally aiming for ~1 µg µl^{-1}).

    ■ **PAUSE POINT** RNA nanoparticles can be stored at −20 °C for ≤6 months or at −80 °C for long-term (>1 year) storage. RNA nanoparticle formation and integrity should be assayed as in Steps 38–40 below before use after long-term storage.

Characterization of 4WJ-drug conjugate nanoparticles and assay drug conjugation

● **TIMING** ~1 month

▲ **CRITICAL** The following assays provide a rather complete characterization of the 4WJ RNA nanoparticles; however, the user may decide that all studies are not necessary for their use. Confirming 4WJ nanoparticle assembly by native PAGE should be done by all users to at least ensure nanoparticle formation and drug conjugation.

Confirmation of 4WJ nanoparticle assembly by 12% (wt/vol) native PAGE in TBE buffer

38. Mix ~250 ng of RNA nanoparticles from Step 37 (including controls such as monomer strands, dimer and trimer intermediates and 4WJ without drug as in Fig. 9a) with 6× running buffer to 1× to generate samples to be loaded into the gel.
39. Prepare and run 12% (wt/vol) native PAGE in TBE buffer of RNA samples at 150 V for 1 h.
40. Stain the gel in ethidium bromide (or an alternative, as above) containing TBE buffer and visualize on a gel imager (e.g., Typhoon FLA 7000 (GE Healthcare)). See Figs. 3b and 9a.

    ◆ **TROUBLESHOOTING**

Nanoparticle size measurement by dynamic light scattering

41. Dissolve RNA nanoparticles in TES buffer to a final concentration of 1 µM. Measure and analyze the hydrodynamic radius of RNA nanoparticles by using a Malvern Zetasizer Nano-SZ at 25 °C and laser wavelength of 633 nm (according to the manufacturer's guideline). See Figs. 3d and 9b,c.

Determination of enzymatic stability and drug release profile

42. Incubate 1 µM preassembled RNA nanoparticles from Step 37 in DMEM cell culture medium containing 50% (vol/vol) FBS (for enzymatic stability) or DEPC-treated water at 37 °C for 0-, 1-, 2-, 4-, 8-, 12-, 18-, 24-, 36- and 48-h time points, flash-freezing each time point on dry ice to halt reactions.
43. Mix each time point with 6× running buffer and load samples into a 3% (wt/vol) agarose gel in TAE buffer containing ethidium bromide (or an alternative, as above). Run the gel at 100 V for 40 min.
44. Visualize on a gel imager and quantify the intensity of each 4WJ band in relation to the 0-h time-point intensity by using ImageJ and plot 4WJ assembly percentage against time.

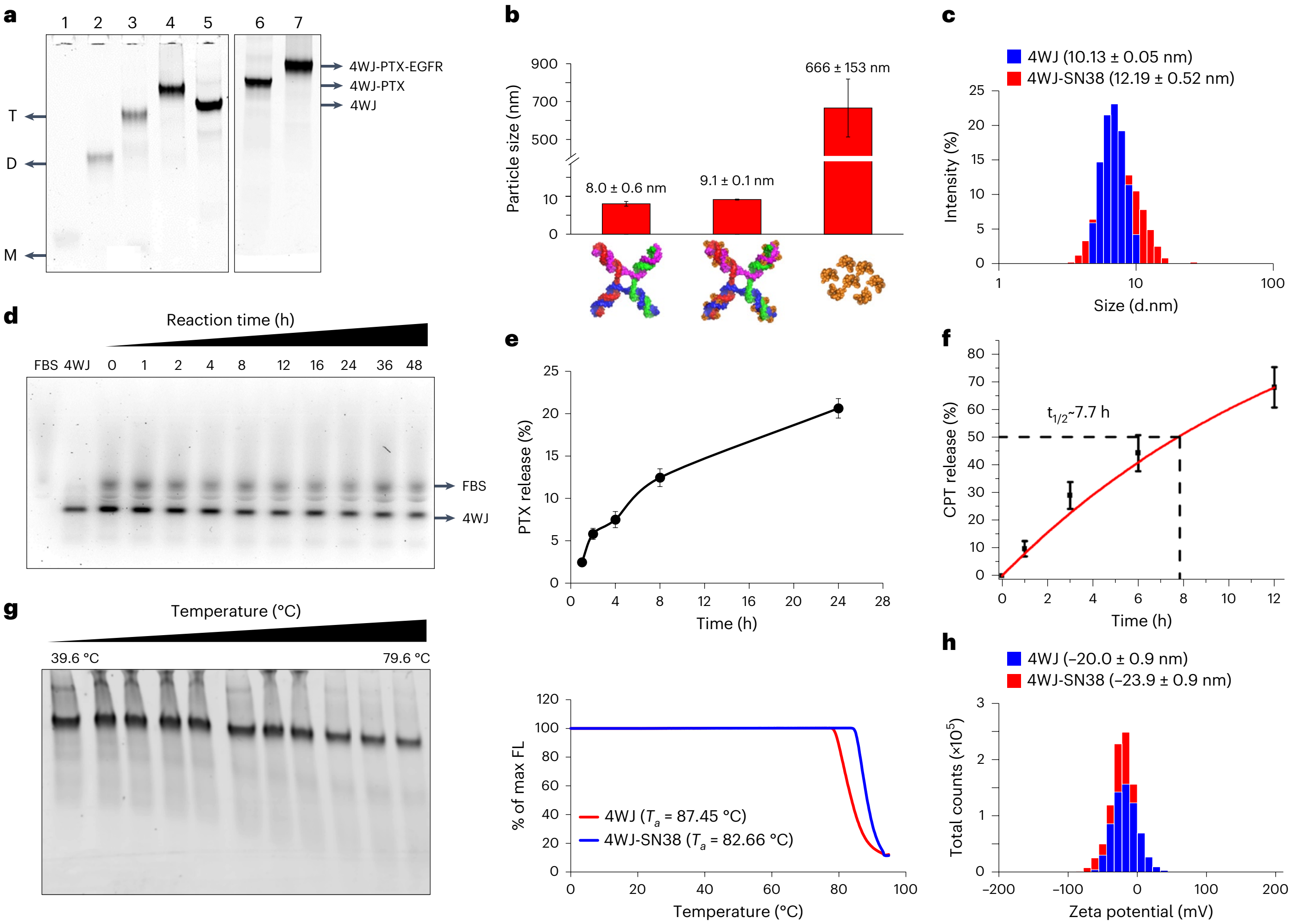

Fig. 9 | Assembly and characterization of 4WJ RNA nanoparticles conjugated with chemotherapeutics. a, Polyacrylamide gel of 4WJ assembly with PTX and EGFR aptamer showing stepwise assembly (1, 4WJ$_A$-6PTX; 2, 4WJ$_{AB}$-12PTX; 3, 4WJ$_{ABC}$-18PTX; 4, 4WJ-24PTX; 5, 4WJ; 6, 4WJ-24PTX; 7, 4WJ-24PTX-EGFR$_{apt}$; M, monomer; D, dimer; T, trimer). **b**,**c**, Size distribution of 4WJ and PTX (**b**) ($n = 3$ presented as average and error bars as s.d.) or SN38 (**c**) by dynamic light scattering. **d**, Polyacrylamide gel analysis of RNA nanoparticle stability after time course serum digestion by FBS. Drug release from the RNA nanoparticle over time exemplified by release of PTX from RNA 6WJ (**e**) and CPT from RNA 3WJ (**f**) ($n = 3$ presented as average and error bars as s.d.). **g**, Thermostability of 4WJ-SN38 demonstrated by TGGE (left) and SYBR Green II fluorescence measured by thermocycler (right). **h**, Zeta potential distribution of 4WJ and 4WJ-SN38. Panel **a** reproduced and panels **b** and **d** adapted from ref. 41, CC BY 4.0 (https://creativecommons.org/licenses/by/4.0/). Panels **c**, **g** and **h** reproduced with permission from ref. 43, Elsevier. Panel **e** reproduced with permission from ref. 34, Elsevier. Panel **f** adapted from ref. 42, CC BY 4.0 (https://creativecommons.org/licenses/by/4.0/).

The nuclease degradation of the RNA nanoparticle will demonstrate a complete decrease in RNA visualized at each time point, while drug release in water from the RNA nanoparticle will demonstrate a more rapid migration rate in the gel.

Determination of nanoparticle T_a by RT-PCR

45. Conduct melting curve experiments by monitoring the fluorescence of the RNA nanoparticles by using the Roche LightCycler 480 real-time PCR system. Add preassembled RNA nanoparticles to a white, round-bottom 96-well plate in TES buffer at a final concentration of 2.5 and 1 µM in 1× SYBR Green II nucleic acid dye (emission: 465–510 nm), which binds double-stranded but not single-stranded nucleic acids.
46. On the Roche LightCycler 480 RT-PCR system, heat the samples to 95 °C for 5 min for the denaturing process, followed by a slow cooling ramp to 20 °C at a rate of 0.11 °C s^{-1} as an

annealing process, while monitoring SYBR Green II emission. Analyze the data with the LightCycler 480 analysis software (according to the manufacturer's instructions) by using the first derivative of the melting profile.

47. Represent annealing curves to show the T_a by using the first derivative of the melting profile (follow the manufacturer's guidelines). Represent the T_m value by using the mean and s.d. from at least three independent experiments.

Determination of nanoparticle T_m by TGGE

▲ **CRITICAL** TGGE allows for the determination of the melting profile and T_m of a single nanoparticle (Fig. 9g, left panel).

48. Mix ~250 ng of RNA sample with 6× running buffer to 1× to generate one sample per well and load the same RNA nanoparticle across each of the 10 wells for the temperature gradient.
49. Run in a 12% (wt/vol) native PAGE in TBE buffer at 100 V for 10 min at RT to allow RNA samples to penetrate into the gel.
50. Transfer the gel to the Biometra TGGE system according to the manufacturer's instructions, with the temperature gradient applied perpendicular to the electrophoresis current. The temperature gradient can be varied, but selecting 30–80 °C provides a wide range to allow calculating the T_m. Run the gel at 20 W for 60 min at RT.
    ▲ **CRITICAL STEP** Elevated temperatures of TGGE can dry the PAGE gel out during electrophoresis. Ensure that electrophoresis wicks properly cover the gel ends and keep the gel hydrated.
51. Stain the gel in ethidium bromide (or an alternative, as above) containing TBE buffer and visualize on a gel imager (i.e., Typhoon FLA 7000 (GE Healthcare)). Quantify the intensity of each 4WJ band in relation to total lane intensity by using ImageJ and plot 4WJ assembly percentage against temperature. The T_m value is defined as the temperature at which 50% of the nanoparticle is dissociated.
    ◆ **TROUBLESHOOTING**

Characterization of the therapeutic effects of 4WJ–drug conjugate nanoparticles in vitro

● **TIMING** ~1 month

▲ **CRITICAL** RNA nanoparticles functionalized with an RNA aptamer allow specific binding and uptake by cancer cells overexpressing the correlating receptor. This binding can be monitored through the use of a fluorescent label (i.e., Alexa Fluor 647) on a component strand of the 4WJ nanoparticle and imaging this fluorophore after incubation with the respective cancer cells. In addition, after binding and cellular internalization, the RNA nanoparticles are able to deliver conjugated chemotherapeutics. The procedures below describe different assays to monitor the targeting of TNBC cells (MDA-MB-231) by an EGFR aptamer on the 4WJ to deliver conjugated PTX[41].

In vitro assay of RNA nanoparticle binding to tumor cells via flow cytometry

52. Maintain MDA-MB-231 cells in DMEM/F-12 culture medium with 10% (vol/vol) FBS and 1% (vol/vol) penicillin-streptomycin. Trypsinize the cells and rinse them with DMEM/F-12 medium without FBS once. Label 4WJ RNA nanoparticles with Alexa647 fluorophore as previously described with 5′-NH_2 modifications and Alexa647-NHS ester[41,70]. Incubate 2×10^5 cells with Alexa647-labeled 4WJ RNA nanoparticles harboring EGFR aptamer or with control RNA nanoparticles not harboring the aptamer, as well as a cell-only control, at 37 °C for 1–4 h in centrifuge tubes. RNA nanoparticles are typically used at 100 nM, but this concentration can be varied.
53. Pellet the cells after 4WJ incubation by centrifuging at 1,000*g* for 5 min at RT and wash the cells with 500 µl of PBS.
54. Repeat pelleting, resuspend the cells in 250 µl of PBS buffer and assay them by flow cytometry using a Biosciences LSRII flow cytometer for Alexa647 (emission: 650 nm; excitation: 665 nm) and following the manufacturer's guidelines.
    ◆ **TROUBLESHOOTING**

In vitro assay of RNA nanoparticle binding to tumor cells via confocal microscopy

55. Maintain MDA-MB-231 cells as described in Step 52. Trypsinize the cells and seed them to 50% confluency on glass coverslips in complete culture medium overnight.
56. Incubate the cells with a 100-nM final concentration of Alexa647-labeled 4WJ RNA nanoparticles harboring EGFR aptamer or with control RNA nanoparticles not harboring the aptamer, as well as a cell-only control, at 37 °C for 4 h.
57. Wash the cells twice with PBS and fix them with 4% (wt/vol) paraformaldehyde at RT for 30 min.
58. Wash the cells with PBS and treat them with 0.1% (vol/vol) Triton X-100 in PBS buffer for 5 min.
59. Wash the cells with PBS and stain them by using Alexa Fluor 488 phalloidin (follow the manufacturer's guidelines) to label the cytoskeleton.
60. Mount the cells by using ProLong gold antifade reagent to stain the nucleus.
61. Assay for aptamer binding and cell entry with an Olympus FV3000 confocal microscope by following the manufacturer's guidelines, imaging each of the three fluorophores. Generate overlay images by using the manufacturer's software to determine nanoparticle binding and internalization.
    ◆ TROUBLESHOOTING

In vitro assay of RNA nanoparticle–induced inhibition of tumor cell proliferation via 3-(4,5-dimethylthiazol-2-yl)-2,5-diphenyltetrazolium bromide (MTT) assay

62. Maintain MDA-MB-231 cells as described in Step 52 above. Trypsinize the cells and seed 5×10^3 cells per well in a 96-well plate overnight in complete culture medium.
63. Incubate 4WJ RNA nanoparticles with and without PTX and/or EGFR aptamer and free PTX into each well in triplicates at indicated concentrations (0.25–24 µM) for 48 h at 37 °C in a humidified 5% CO_2 incubator.
64. Using the Promega CellTiter 96 non-radioactive cell proliferation assay, follow the manufacturer's guidelines, adding 15 µl of MTT dye solution to each well and incubate at 37 °C in the dark for 4 h.
65. Add 50 µl of solubilization solution/stop mix to stop the dye solution reaction and solubilize the formed crystals until the solution is uniformly colored.
66. Measure the absorbance of each well at 570 nm by using a plate reader (Bio-Tek Synergy 4), averaging the triplicate samples. Normalize absorbance to the cell-only sample to estimate cell proliferation inhibition caused by PTX release from the RNA nanoparticles.

In vitro assay to measure RNA nanoparticle–induced apoptosis of tumor cells via Annexin V/propidium iodide staining

67. Maintain MDA-MB-231 cells as described in Step 52 above. Trypsinize the cells, seed 5×10^4 cells per well in a 24-well plate overnight at 37 °C and culture them in a 5% CO_2 humidified incubator.
68. Incubate the cells with 4WJ RNA nanoparticles with and without PTX and/or EGFR aptamer and free PTX at a final concentration of 1 µM PTX for 24 h at 37 °C in a humidified 5% CO_2 incubator.
69. Trypsinize the cells into suspension, wash in PBS buffer twice and suspend them in 100 µl of 1× Annexin V-FITC binding buffer by using the BD Pharmingen FITC Annexin V apoptosis detection kit. Add 5 µl of Annexin V-FITC followed by 5 µl of propidium iodide to each well and incubate at RT for 20 min.
70. Transfer the samples to tubes for flow cytometry with 200 µl of 1× binding buffer and assay the samples by flow cytometry using a Biosciences LSRII flow cytometer and following the manufacturer's guidelines.

In vitro assay of RNA nanoparticle–induced cytokine response

71. RAW 264.7 macrophage cells are commonly used to examine cytokine induction and release. Maintain RAW 264.7 cells in DMEM full growth medium with 10% (vol/vol) FBS.

Distribute aliquots of 5×10^4 cells per well into a 24-well plate and culture at 37 °C overnight in a humidified 5% CO_2 incubator.

72. Add 4WJ RNA nanoparticles (100 nM) and lipopolysaccharide (5.5 μg ml^{-1}, 100 nM final concentration) per well of RAW 264.7 cells in 200 μl of Opti-MEM cell medium and incubate at 37 °C for 16 h.
73. Collect the supernatants of cell medium and freeze at −80 °C for further analysis. The TNF and IL-6 in diluted supernatants were measured by mouse ELISA MAX deluxe sets and following the manufacturer's protocols.

Troubleshooting

Troubleshooting advice can be found in Table 2.

Table 2 | Troubleshooting table

Step	Problem	Possible reason	Solution
13	Low yield in RNA oligo synthesis	Water contamination in phosphoramidites or solvents	Use new solvents that have been dehydrated through the use of molecular sieves and degassed, and dissolve all phosphoramidites in a dry environment (i.e., under argon gas)
		Inert gas supply (argon or helium) has too high humidity	Check with the gas supplier on humidity levels of gases and purchase low-humidity inert gas or include an inline desiccant column
		Low gas (argon or helium) pressure	Check the system for gas leaks and complete preventative maintenance to the Biosset ASM-800 synthesizer according to the manufacturer's recommendations
18	Low yield in prodrug formation	The reaction time is too short	Extend the reaction time
		Water contamination in the reaction	Ensure that the reaction is done under a dry environment (i.e., in argon gas) or use molecular sieves to absorb water
		The reaction needs additional catalysis	Replace DCC with EDC in the reaction
22(A)xv	The NMR signal of the azide-conjugated prodrug is obscured by impurities	Presence of unreacted linker or unconjugated prodrug, resulting in overlap with prodrug signals	Complete additional column chromatography to remove reactants
		Presence of trace amounts of ethyl acetate, dichloromethane or methanol solvents in the samples	Thoroughly dry the samples either under vacuum for 12 h or by using a Schlenk line for several hours before running NMR
		The presence of moisture or residual water can result in a broad peak from 3.0 to 3.5 p.p.m. in $CDCl_3$	
29	Poor recovery of RNA after ethanol precipitation	RNA not fully eluted from the gel pieces	Extend the elution time at 37 °C or cut the gel into smaller pieces to encourage buffer exchange and repeat the elution
		Incorrect final concentration of ethanol, preventing RNA precipitation	Ensure that the solution has ≥70% (vol/vol) ethanol. RNA will not precipitate at lower ethanol concentrations
		Too low concentration of RNA	Reduce the total volumes of elution buffer during gel elution to increase RNA concentrations, thus promoting aggregation
31	Low reaction yield in prodrug conjugation to RNA oligo	Low concentration of Cu^{1+} ions in the reaction	Ensure that the CuBr solution is freshly prepared
			Ensure a proper CuBr-to–ascorbic acid ratio or increase the ratio of ascorbic acid to CuBr to ensure that Cu^{2+} is converted to Cu^{1+}
		The reaction is turbid, and prodrug is not dissolved	Increase the concentration of click solvent, heat the reaction to 37 °C or sonicate the reaction. Note: prolonged exposure to heat may promote RNA degradation
40	Low yield of 4WJ nanoparticle formation	Incorrect Mg^{2+} concentration	Excessive Mg^{2+} concentration can promote nanoparticle aggregation. Change the buffer composition to reduce Mg^{2+} concentrations
		Incorrect molar ratios of RNA oligos	If by-product (trimer, dimer or monomer) bands are seen in the gel, equal molar mixing of RNA oligos was not achieved, and the concentrations of oligo strands should be checked
51	Uneven migration rates during TGGE	Drying of the gel and buffer wicks due to the gel-heating gradient	Ensure that the wicks are saturated with buffer, are submerged in buffer chambers and have proper overlap with the gel, to prevent drying

Table 2 (continued) | Troubleshooting table

Step	Problem	Possible reason	Solution
54, 61	Poor cancer cell binding	The concentration of RNA nanoparticle used is too low	Increase the concentration of RNA nanoparticle incubated with the cell (i.e., 250 nM)
		The incubation time of RNA nanoparticles with the cells is too long or short	Increase the incubation time of RNA nanoparticles with the cells if too little binding is seen
			Decrease the incubation time of RNA nanoparticles with the cells if the no-ligand control shows too high of binding with the cells

Timing

Steps 1–13, synthesis of 4WJ component strand oligos: ~1 week
Steps 14–22, chemical synthesis of a chemotherapeutic prodrug: ~1 week
Steps 23–31, conjugation of prodrug-azide to 4WJ component strand via click chemistry: 4–5 d
Steps 32–37, assembly of ultra-stable 4WJ RNA nanoparticles harboring chemotherapeutics: 2–3 d
Steps 38–51, characterization of 4WJ-drug conjugate nanoparticles and assay drug conjugation: ~1 month
Steps 52–73, characterization of 4WJ-drug conjugate nanoparticles for therapeutic effect in vitro: ~1 month

Anticipated results

This protocol provides detailed procedures for the design and construction of multifunctional, stable RNA nanoparticles capable of selectively targeting solid tumors and conjugating up to 24 molecules of chemotherapeutic drugs, including PTX, SN38 and CPT. We also provide methodology for characterizing the RNA nanoparticles and assaying for in vitro cancer cell proliferation inhibition and toxicity. The inclusion of a tumor targeting ligand (e.g., EGFR aptamer), inclusion of a fluorophore (e.g., Alexa Fluor 647) and conjugation of the chemotherapeutic drug occur before final assembly of the 4WJ RNA nanoparticle through RNA synthesis and click chemistry reactions. The chemical reactions for chemotherapeutic modification and conjugation to the RNA were selected for their relative high yield and easy purification from by-products. The anticipated results of this protocol are described below.

4WJ RNA nanoparticles are highly thermodynamically (Fig. 3e) and chemically stable (Fig. 9d) and form into homogeneous nanocomplexes (expected to have a hydrodynamic size of about 10 nm) (Fig. 3d and Fig. 9c). The 4WJ nanoparticle is designed to have a high thermodynamic stability through strong base pairing of component strands that are not interrupted by the conjugation of hydrophobic chemical drugs[41] (Fig. 3e, right panel). In addition, the pRNA-3WJ, which served as the basis for designing the 4WJ, has shown strong stability against chemical denaturation, including 8 M urea[57]. Upon the inclusion of 2′-fluoro modifications to pyrimidine nucleotides during chemical synthesis, the RNA nanoparticle is resistant to nuclease cleavage and degradation[41,57,190,214]. The base pairing of the 4WJ allows for specific interactions of component strands that result in controlled stoichiometry, generating a homogeneous product (Fig. 3b,c).

The synthesis of RNA component strands using a 1-μmol scale universal support column should produce about 4 mg of each RNA strand. If concentrations of RNA strands are substantially less, the most common cause is either a pressure leak within the synthesizer, causing volumes to be inaccurately pumped across the support column, or water contaminants in the phosphoramidite or solutions used during the synthesis. Users should check that all bottles are tightly fitted onto the synthesizer and that pressure is maintained during the entire synthesis. If water is the cause of low yield, solvents can be dried, and molecular sieves can be used to absorb any water present. To monitor the yield of each nucleotide addition on the support column, users should check for a vibrant orange color across the column, indicating deprotection of each nucleotide (Step 3(iv)) and release of DMT. During purification of chemotherapeutic conjugated RNA component strands by HPLC, a high yield (>90%) of total RNA should be recovered, whereas gel purification results in a lower (about 75%) final yield because of inefficiencies in gel elution. If low yields are seen in HPLC purification, it is most probably because of poor RNA adhesion to the column due to improper column conditioning. Users should recheck the equipment setup protocol. If a large amount of RNA is lost by gel purification, issues could be due to poor gel elution yield or poor ethanol precipitation conditions. Users must make sure that RNA samples are precipitated by using 70% (vol/vol) ethanol for maximum efficiency. Gel elution can be improved through repeated elutions, a longer elution time or cutting the gel piece into smaller pieces to promote buffer exchange.

Because of the reactive hydroxyl groups on the suggested chemotherapeutics here, azide linkers can be incorporated onto the small molecule drugs to generate prodrugs that are conjugatable to RNA nanoparticles. Successful modification of these chemotherapeutics can be confirmed by ^{1}H-NMR and mass spectrometry. Conjugation of the azide linker (6-azidohexanoic acid) to form the prodrug is confirmed by the appearance of the new peak in the aliphatic region (2–5 p.p.m.) of the ^{1}H-NMR (Fig. 7a). The 6-azidohexanoic acid moiety shows two distinct triplets (with integration of 2H each) corresponding to a methylene proton adjacent to the N_3 and ester groups. The ester group appears slightly downfield (shift to higher p.p.m.) because of deshielding by the electronegative ester group compared to another triplet that is adjacent to the azide. A quintet (2H) is observed for the central methylene protons, and a multiplet (4H) corresponds to the two internal methylene groups between the terminal triplets and quintet. The ^{1}H-NMR spectrum can also be used for assessing the purity of the azide-conjugated prodrug. Successful conjugation is also confirmed by the disappearance of the carboxylic acid signal from 6-azidohexanoic acid, indicating ester bond formation. The free carboxylic acid typically appears as a small, broad peak around 10–12 p.p.m. in the ^{1}H NMR spectrum. Upon conjugation, this peak disappears due to esterification. The carboxylic acid proton is exchangeable with water or moisture in deuterated solvents, which can cause the peak to broaden or become undetectable.

The 4WJ RNA nanoparticle with inclusion of 2′-alkyne modifications results in specific conjugation of chemotherapeutic prodrugs[34,41–43,64] (Fig. 8). The resulting conjugates do not allow for aggregation of chemical drugs or interference with nanoparticle complexation. The 4WJ has been designed to space chemical drug conjugates to prevent these two issues, while having a high yield of conjugation. In addition, the conjugation of hydrophobic drugs to the RNA 4WJ results in substantial water solubility of the drugs (Fig. 8, right panel).

The 4WJ RNA nanoparticle is designed so that base pairing of component strands allows for formation only into >10-nm nanoparticles (Fig. 3d and Fig. 9c), and generally nanoparticles do not form aggregates or larger particles. The conjugation of chemical drugs, if spaced properly (≥5 nt between each drug), will not promote aggregation of the nanoparticle. Temporary aggregation of the RNA 4WJ may be seen if buffers have a high Mg^{2+} concentration (>10 mM). The aggregation can be broken back to individual nanoparticles by removing Mg^{2+} via EDTA addition or buffer dialysis.

Conjugated chemotherapeutics are cleavable by esterase or hydrolysis of the ester, allowing for stable conjugation and controlled release in the tumor environment. As shown in Fig. 9e,f, drug release has a half-life of about 8 h in FBS, which mimics in vivo circulation and aligns well with the time it takes for RNA nanoparticles to reach the tumor environment[34,42,215]. In addition, upon cleaving of the ester linker, the chemotherapeutic returns to its original structure and function, demonstrating strong tumor inhibition[34,41–43], while improving upon the safety profile of the otherwise toxic chemotherapeutic[41,44]. Because of the water sensitivity of the ester linker, it is important to store the 4WJ-drug conjugate at −20 °C for short-term storage (>6 months) and at −80 °C for long-term storage. This will prevent hydrolysis of the ester linker and ensure that the RNA nanoparticle retains its chemotherapeutic conjugates long term. The high thermostability of the RNA 4WJ allows for storage in water or various buffers without concern of RNA nanoparticle dissociation. In general though, esters are sensitive to changes

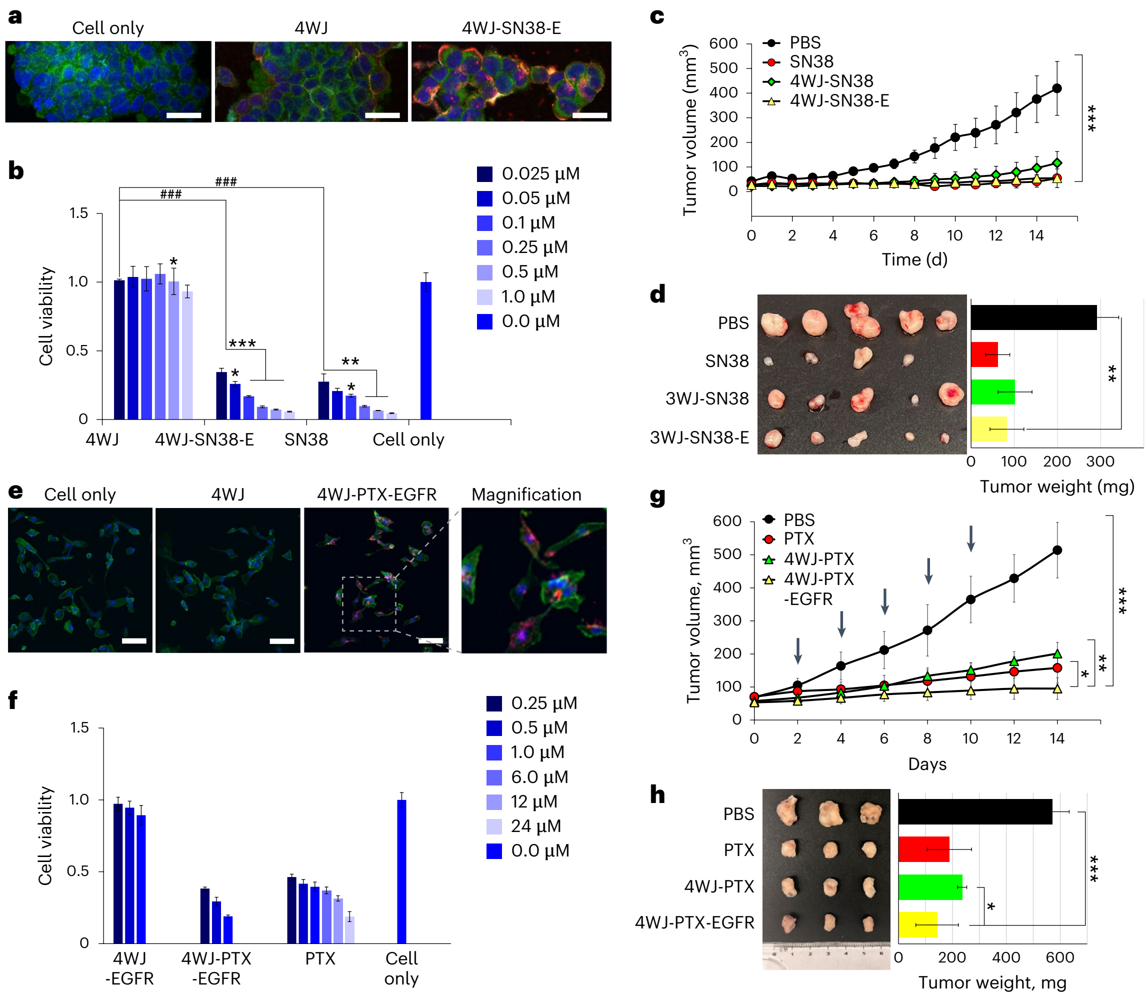

Fig. 10 | Efficacy of drug-conjugated 4WJ nanoparticles for treatment of cancer. a,**e**, Cell targeting and internalization of 4WJ-SN38-EpCAM for treatment of HT29 colorectal cancer cells (**a**) and 4WJ-PTX-EGFR treatment of MDA-MB-231 TNBC cells (**e**) by confocal microscopy (scale bars, 100 µm; blue, nucleus; green, cytososkelton; red, RNA nanoparticle). **b**,**f**, Cell proliferation inhibition assessed by MTT assay of HT29 (**b**) or MDA-MB-231 (**f**) cells ($n = 3$ presented as average and error bars as s.d.). **c**,**g**, Tumor volume measured during tumor treatment by naked chemotherapeutic or RNA nanoparticles delivering chemotherapeutics, for SN38 (**c**) and PTX (**g**) ($n = 5$ mice, presented as average and error bars as s.e.m. for **c** or s.d. for **g**). **d**,**h**, Tumor images and tumor weights at the conclusion of treatment, for SN38 (**d**) and PTX (**h**) ($n = 5$ presented as average and error bars as s.e.m. for **d** or s.d. for **h**). Panels **a**–**c** reproduced and panel **d** adapted with permission from ref. 43, Elsevier. Panel **e** reproduced and panels **f**–**h** adapted from ref. 41, CC BY 4.0 (https://creativecommons.org/licenses/by/4.0/).

in pH and elevated temperatures. Therefore, storage buffers should maintain a neutral pH. Thermostability studies on TGGE did not show immediate PTX release from the RNA 4WJ at 80 °C during the 1 h it took to run the gel[41], suggesting overall stability of the drug conjugate.

Inclusion of targeting RNA aptamers, such as EGFR[41], EpCAM[43] or prostate-specific membrane antigen[29], on the RNA nanoparticle results in specific cellular uptake by cells expressing the respective receptor (Fig. 10a,e). It is expected that flow cytometry and confocal microscopy will demonstrate selective uptake of targeted nanoparticles over control nanoparticles without the aptamer. As a result of cellular uptake of 4WJ-drug conjugates, prodrugs are cleaved in the endosome, and drugs are released into the cytoplasm. Cell viability assays demonstrate the controlled inhibition of colorectal cell proliferation by SN38 delivery (Fig. 10b) and TNBC cell proliferation by PTX delivery (Fig. 10f). Finally, when delivered intravenously into mice harboring tumors, RNA nanoparticles demonstrate significant tumor growth inhibition compared to controls (Fig. 10c,g), with tumors showing significant differences in weight (Fig. 10d,h).

Data availability

Data that support this Protocol can be found in their original publications[34,41–43,64] and are included as Supplementary Data.

Received: 3 March 2025; Accepted: 5 November 2025;
Published online: 03 February 2026

References

1. Singla, A. K., Garg, A. & Aggarwal, D. Paclitaxel and its formulations. *Int. J. Pharm.* **235**, 179–192 (2002).
2. Liu, S. Q., Wiradharma, N., Gao, S. J., Tong, Y. W. & Yang, Y. Y. Bio-functional micelles self-assembled from a folate-conjugated block copolymer for targeted intracellular delivery of anticancer drugs. *Biomaterials* **28**, 1423–1433 (2007).
3. De Jong, W. H. & Borm, P. J. Drug delivery and nanoparticles: applications and hazards. *Int. J. Nanomed.* **3**, 133–149 (2008).
4. Kouchakzadeh, H., Safavi, M. S. & Shojaosadati, S. A. Efficient delivery of therapeutic agents by using targeted albumin nanoparticles. *Adv. Protein Chem. Struct. Biol.* **98**, 121–143 (2015).
5. McNeil, S. E. Nanoparticle therapeutics: a personal perspective. *Wiley Interdiscip. Rev. Nanomed. Nanobiotechnol.* **1**, 264–271 (2009).
6. Desai, N. Challenges in development of nanoparticle-based therapeutics. *AAPS J.* **14**, 282–295 (2012).
7. Hafeez, U., Parakh, S., Gan, H. K. & Scott, A. M. Antibody-drug conjugates for cancer therapy. *Molecules* **25**, 4764 (2020).
8. Tarantino, P. et al. Antibody-drug conjugates: smart chemotherapy delivery across tumor histologies. *CA Cancer J. Clin.* **72**, 165–182 (2022).
9. Dean, A. Q., Luo, S., Twomey, J. D. & Zhang, B. Targeting cancer with antibody-drug conjugates: promises and challenges. *MAbs* **13**, 1951427 (2021).
10. Maiti, R. et al. Antibody drug conjugates as targeted cancer therapy: past development, present challenges and future opportunities. *Arch. Pharm. Res.* **46**, 361–388 (2023).
11. Guo, P. X., Erickson, S. & Anderson, D. A small viral RNA is required for in vitro packaging of bacteriophage ϕ29 DNA. *Science* **236**, 690–694 (1987).
12. Guo, P., Zhang, C., Chen, C., Garver, K. & Trottier, M. Inter-RNA interaction of phage ϕ29 pRNA to form a hexameric complex for viral DNA transportation. *Mol. Cell* **2**, 149–155 (1998).
13. Guo, P. The emerging field of RNA nanotechnology. *Nat. Nanotechnol.* **5**, 833–842 (2010).
14. Shu, Y. et al. Stable RNA nanoparticles as potential new generation drugs for cancer therapy. *Adv. Drug Deliv. Rev.* **66**, 74–89 (2014).
15. Pardi, N., Hogan, M. J., Porter, F. W. & Weissman, D. mRNA vaccines—a new era in vaccinology. *Nat. Rev. Drug Discov.* **17**, 261–279 (2018).
16. Corbett, K. S. et al. SARS-CoV-2 mRNA vaccine design enabled by prototype pathogen preparedness. *Nature* **586**, 567–571 (2020).
17. Jackson, L. A. et al. An mRNA vaccine against SARS-CoV-2—preliminary report. *N. Engl. J. Med.* **383**, 1920–1931 (2020).
18. Hoy, S. M. Patisiran: first global approval. *Drugs* **78**, 1625–1631 (2018).
19. Binzel, D. W. et al. Thermostability, tunability, and tenacity of RNA as rubbery anionic polymeric materials in nanotechnology and nanomedicine-specific cancer targeting with undetectable toxicity. *Chem. Rev.* **121**, 7398–7467 (2021).
20. Ghimire, C. et al. RNA nanoparticles as rubber for compelling vessel extravasation to enhance tumor targeting and for fast renal excretion to reduce toxicity. *ACS Nano* **14**, 13180–13191 (2020).
21. Li, X., Bhullar, A. S., Binzel, D. W. & Guo, P. The dynamic, motile and deformative properties of RNA nanoparticles facilitate the third milestone of drug development. *Adv. Drug Deliv. Rev.* **186**, 114316 (2022).
22. Guo, P. RNA nanotechnology: engineering, assembly and applications in detection, gene delivery and therapy. *J. Nanosci. Nanotechnol.* **5**, 1964–1982 (2005).
23. Ni, X., Castanares, M., Mukherjee, A. & Lupold, S. E. Nucleic acid aptamers: clinical applications and promising new horizons. *Curr. Med. Chem.* **18**, 4206–4214 (2011).
24. Thiviyanathan, V. & Gorenstein, D. G. Aptamers and the next generation of diagnostic reagents. *Proteom. Clin. Appl.* **6**, 563–573 (2012).
25. Kang, K. N. & Lee, Y. S. RNA aptamers: a review of recent trends and applications. *Adv. Biochem. Eng. Biotechnol.* **131**, 153–169 (2013).
26. Xu, C. et al. Conversion of chemical drugs into targeting ligands on RNA nanoparticles and assessing payload stoichiometry for optimal biodistribution in cancer treatment. *RNA Nanomed.* **1**, 109–123 (2024).
27. Binzel, D. W. et al. RNA nanoparticles harboring radioisotopes or other imaging molecules for spontaneous tumor targeting for early cancer diagnosis. *RNA Nanomed.* **2**, 10.59566/isrnn.2025.0201d (2025).
28. Shu, Y., Cinier, M., Shu, D. & Guo, P. Assembly of multifunctional phi29 pRNA nanoparticles for specific delivery of siRNA and other therapeutics to targeted cells. *Methods* **54**, 204–214 (2011).
29. Binzel, D. et al. Specific delivery of miRNA for high efficient inhibition of prostate cancer by RNA nanotechnology. *Mol. Ther.* **24**, 1267–1277 (2016).
30. Xu, Y. et al. Specific delivery of delta-5-desaturase siRNA *via* RNA nanoparticles supplemented with dihomo-γ-linolenic acid for colon cancer suppression. *Redox Biol.* **21**, 101085–101093 (2019).
31. Yang, L., Li, Z., Binzel, D. W., Guo, P. & Williams, T. M. Targeting oncogenic KRAS in non-small cell lung cancer with EGFR aptamer-conjugated multifunctional RNA nanoparticles. *Mol. Ther. Nucleic Acids* **33**, 559–571 (2023).
32. Shu, D. et al. Systemic delivery of anti-miRNA for suppression of triple negative breast cancer utilizing RNA nanotechnology. *ACS Nano* **9**, 9731–9740 (2015).
33. Yin, H. et al. Delivery of anti-miRNA for triple-negative breast cancer therapy using RNA nanoparticles targeting stem cell marker CD133. *Mol. Ther.* **27**, 1252–1261 (2019).
34. Wang, H. et al. Multivalent rubber-like RNA nanoparticles for targeted co-delivery of paclitaxel and MiRNA to silence the drug efflux transporter and liver cancer drug resistance. *J. Control. Release* **330**, 173–184 (2020).
35. Bian, H. et al. CD133-guided RNA nanoparticle delivery of FTO siRNA impairs leukemia resistance to tyrosine kinase inhibitor therapy. *RNA Nanomed.* **2**, 70–88 (2025).
36. Beasock, D. et al. The reduction of traumatic spinal cord secondary injury by anti-RhoA siRNA functionalized nucleic acid nanoparticles (NANPs). *RNA Nanomed.* **1**, 79–90 (2024).
37. Jasinski, D. L., Yin, H., Li, Z. & Guo, P. Hydrophobic effect from conjugated chemicals or drugs on in vivo biodistribution of RNA nanoparticles. *Hum. Gene Ther.* **29**, 77–86 (2018).
38. Jasinski, D. L., Li, H. & Guo, P. The effect of size and shape of RNA nanoparticles on biodistribution. *Mol. Ther.* **26**, 784–792 (2018).
39. Wang, H. & Guo, P. Radiolabeled RNA nanoparticles for highly specific targeting and efficient tumor accumulation with favorable in vivo biodistribution. *Mol. Pharm.* **18**, 2924–2934 (2021).
40. Grabow, W. W. & Jaeger, L. RNA self-assembly and RNA nanotechnology. *Acc. Chem. Res.* **47**, 1871–1880 (2014).
41. Guo, S. et al. Ultra-thermostable RNA nanoparticles for solubilizing and high-yield loading of paclitaxel for breast cancer therapy. *Nat. Commun.* **11**, 972–982 (2020).
42. Piao, X., Yin, H., Guo, S., Wang, H. & Guo, P. RNA nanotechnology to solubilize ydrophobic antitumor drug for targeted delivery. *Adv. Sci.* **6**, 1900951 (2019).
43. Li, X. et al. RNA four-way junction (4WJ) for spontaneous cancer-targeting, effective tumor-regression, metastasis suppression, fast renal excretion and undetectable toxicity. *Biomaterials* **305**, 122432 (2023).
44. Jin, K. et al. In vitro and in vivo evaluation of the pathology and safety aspects of three- and four-way junction RNA nanoparticles. *Mol. Pharm.* **21**, 718–728 (2024).
45. Che, Y. et al. Targeting EGFR self-assembling RNA nanoparticles co-delivering paclitaxel and miRNA21 inhibitors for the treatment of head and neck tumors *RNA*. *Nanomed* **2**, 33–51 (2025).
46. Jasinski, D., Haque, F., Binzel, D. W. & Guo, P. Advancement of the emerging field of RNA nanotechnology. *ACS Nano* **11**, 1142–1164 (2017).
47. Afonin, K. A. et al. Multifunctional RNA nanoparticles. *Nano Lett.* **14**, 5662–5671 (2014).
48. Kim, J. & Franco, E. RNA nanotechnology in synthetic biology. *Curr. Opin. Biotechnol.* **63**, 135–141 (2020).
49. Piao, X., Wang, H., Binzel, D. W. & Guo, P. Assessment and comparison of Thermal stability of phosphorothioate-DNA, DNA, RNA, 2′-F RNA, and LNA in the context of Phi29 pRNA 3WJ. *RNA* **24**, 67–76 (2018).
50. Huang, L. C. et al. Nicotinic acetylcholine receptor subtype alpha-9 mediates triple-negative breast cancers based on a spontaneous pulmonary metastasis mouse model. *Front. Cell. Neurosci.* **11**, 336 (2017).
51. Khisamutdinov, E. F. et al. Enhancing immunomodulation on innate immunity by shape transition among RNA triangle, square and pentagon nanovehicles. *Nucleic Acids Res.* **42**, 9996–10004 (2014).
52. Guo, S. et al. Size, shape, and sequence-dependent immunogenicity of RNA nanoparticles. *Mol. Ther. Nucleic Acids* **9**, 399–408 (2017).
53. Rackley, L. et al. RNA fibers as optimized nanoscaffolds for siRNA coordination and reduced immunological recognition. *Adv. Funct. Mater.* **28**, 1805959 (2018).
54. Chandler, M. & Afonin, K. A. Smart-responsive nucleic acid nanoparticles (NANPs) with the potential to modulate immune behavior. *Nanomaterials* **9**, 611 (2019).
55. Guo, S., Tschammer, N., Mohammed, S. & Guo, P. Specific delivery of therapeutic RNAs to cancer cells via the dimerization mechanism of phi29 motor pRNA. *Hum. Gene Ther.* **16**, 1097–1109 (2005).

56. Shu, Y., Cinier, M., Fox, S. R., Ben-Johnathan, N. & Guo, P. Assembly of therapeutic pRNA-siRNA nanoparticles using bipartite approach. *Mol. Ther.* **19**, 1304–1311 (2011).
57. Shu, D., Shu, Y., Haque, F., Abdelmawla, S. & Guo, P. Thermodynamically stable RNA three-way junction for constructing multifunctional nanoparticles for delivery of therapeutics. *Nat. Nanotechnol.* **6**, 658–667 (2011).
58. Sharma, A. et al. Controllable self-assembly of RNA dendrimers. *Nanomedicine* **12**, 835–844 (2016).
59. Li, H. et al. Construction of RNA nanotubes. *Nano Res.* **12**, 1952–1958 (2019).
60. Li, H. et al. RNA nanotechnology to build a dodecahedral genome of single-stranded RNA virus. *RNA Biol.* **18**, 2390–2400 (2021).
61. Jasinski, D. L., Khisamutdinov, E. F., Lyubchenko, Y. L. & Guo, P. Physicochemically tunable polyfunctionalized RNA square architecture with fluorogenic and ribozymatic properties. *ACS Nano* **8**, 7620–7629 (2014).
62. Khisamutdinov, E. F., Jasinski, D. L. & Guo, P. RNA as a boiling-resistant anionic polymer material to build robust structures with defined shape and stoichiometry. *ACS Nano* **8**, 4771–4781 (2014).
63. Khisamutdinov, E. F. et al. Simple method for constructing RNA triangle, square, pentagon by tuning interior RNA 3WJ angle from 60 degrees to 90 degrees or 108 degrees. *Methods Mol. Biol.* **1316**, 181–193 (2015).
64. Shu, Y. et al. RNA-based micelles: a novel platform for paclitaxel loading and delivery. *J. Control. Release* **276**, 17–29 (2018).
65. Shopsowitz, K. E., Roh, Y. H., Deng, Z. J., Morton, S. W. & Hammond, P. T. RNAi-microsponges form through self-assembly of the organic and inorganic products of transcription. *Small* **10**, 1623–1633 (2014).
66. Bui, M. N. et al. Versatile RNA tetra-U helix linking motif as a toolkit for nucleic acid nanotechnology. *Nanomedicine* **13**, 1137–1146 (2017).
67. Zakrevsky, P. et al. Truncated tetrahedral RNA nanostructures exhibit enhanced features for delivery of RNAi substrates. *Nanoscale* **12**, 2555–2568 (2020).
68. Lin, Y. X. et al. RNA nanotechnology-mediated cancer immunotherapy. *Theranostics* **10**, 281–299 (2020).
69. Jaeger, L., Westhof, E. & Leontis, N. B. TectoRNA: modular assembly units for the construction of RNA nano-objects. *Nucleic Acids Res.* **29**, 455–463 (2001).
70. Shu, Y., Shu, D., Haque, F. & Guo, P. Fabrication of pRNA nanoparticles to deliver therapeutic RNAs and bioactive compounds into tumor cells. *Nat. Protoc.* **8**, 1635–1659 (2013).
71. Shu, Y. et al. Fabrication of 14 different RNA nanoparticles for specific tumor targeting without accumulation in normal organs. *RNA* **19**, 767–777 (2013).
72. Lee, T. J. et al. RNA nanoparticle as a vector for targeted siRNA delivery into glioblastoma mouse model. *Oncotarget* **6**, 14766–14776 (2015).
73. Cui, D. et al. Regression of gastric cancer by systemic injection of RNA nanoparticles carrying both ligand and siRNA. *Sci. Rep.* **5**, 10726–10739 (2015).
74. Rychahou, P. et al. Delivery of RNA nanoparticles into colorectal cancer metastases following systemic administration. *ACS Nano* **9**, 1108–1116 (2015).
75. Zhang, Y. et al. Overcoming tamoxifen resistance of human breast cancer by targeted gene silencing using multifunctional pRNA nanoparticles. *ACS Nano* **11**, 335–346 (2017).
76. Lee, T. J. et al. RNA nanoparticle-based targeted therapy for glioblastoma through inhibition of oncogenic miR-21. *Mol. Ther.* **25**, 1544–1555 (2017).
77. Pang, L. et al. EpCAM-targeted 3WJ RNA nanoparticle harboring delta-5-desaturase siRNA inhibited lung tumor formation via DGLA peroxidation. *Mol. Ther. Nucleic Acids* **22**, 222–235 (2020).
78. Beaucage, S. L. & Caruthers, M. H. Deoxynucleoside phosphoramidites—a new class of key intermediates for deoxypolynucleotide synthesis. *Tetrahedron Lett.* **22**, 1859–1862 (1981).
79. Beaucage, S. L. & Iyer, R. P. Advances in the synthesis of oligonucleotides by the phosphoramidite approach. *Tetrehedron* **48**, 2223–2311 (1992).
80. Flemmich, L., Bereiter, R. & Micura, R. Chemical synthesis of modified RNA. *Angew. Chem. Int. Ed. Engl.* **63**, e202403063 (2024).
81. Brown, D. M. A brief history of oligonucleotide synthesis. *Methods Mol. Biol.* **20**, 1–17 (1993).
82. Kolb, H. C., Finn, M. G. & Sharpless, K. B. Click chemistry: diverse chemical function from a few good reactions. *Angew. Chem. Int. Ed. Engl.* **40**, 2004–2021 (2001).
83. Brown, T. & Norden, B. Nobel Prize 2022 to Sharpless, Meldal, Bertozzi Click Chemistry - molecular lego. *Q. Rev. Biophys.* **55**, e13 (2022).
84. Huisgen, R. Centenary lecture - 1,3-dipolar cycloadditions. *Proc. Chem. Soc*. 357–396 (1961).
85. Diamond, J. M., Turner, D. H. & Mathews, D. H. Thermodynamics of three-way multibranch loops in RNA. *Biochemistry* **40**, 6971–6981 (2001).
86. Zhang, H. et al. Crystal structure of 3WJ core revealing divalent ion-promoted thermostability and assembly of the Phi29 hexameric motor pRNA. *RNA* **19**, 1226–1237 (2013).
87. Jedrzejczyk, D. & Chworos, A. Self-assembling RNA nanoparticle for gene expression regulation in a model system. *ACS Synth. Biol.* **8**, 491–497 (2019).
88. Duckett, D. R., Murchie, A. I. & Lilley, D. M. The global folding of four-way helical junctions in RNA, including that in U1 snRNA. *Cell* **83**, 1027–1036 (1995).
89. Haque, F. et al. Ultrastable synergistic tetravalent RNA nanoparticles for targeting to cancers. *Nano Today* **7**, 245–257 (2012).
90. Severcan, I., Geary, C., Verzemnieks, E., Chworos, A. & Jaeger, L. Square-shaped RNA particles from different RNA folds. *Nano Lett.* **9**, 1270–1277 (2009).
91. Dibrov, S. M., McLean, J., Parsons, J. & Hermann, T. Self-assembling RNA square. *Proc. Natl Acad. Sci. USA.* **108**, 6405–6408 (2011).
92. Sharan, R., Bindewald, E., Kasprzak, W. K. & Shapiro, B. A. Computational generation of RNA nanorings. *Methods Mol. Biol.* **1632**, 19–32 (2017).
93. Oi, H. et al. Programmable formation of catalytic RNA triangles and squares by assembling modular RNA enzymes. *J. Biochem.* **161**, 451–462 (2017).
94. Li, H. et al. Controllable self-assembly of RNA tetrahedrons with precise shape and size for cancer targeting. *Adv. Mater.* **28**, 7501–7507 (2016).
95. Purzycka, K. J. et al. Automated 3D RNA structure prediction using the RNAComposer method for riboswitches. *Methods Enzymol.* **553**, 3–34 (2015).
96. Khisamutdinov, E. F. et al. Fabrication of RNA 3D nanoprisms for loading and protection of small RNAs and model drugs. *Adv. Mater.* **28**, 10079–10087 (2016).
97. Yin, H., Wang, H., Li, Z., Shu, D. & Guo, P. RNA micelles for the systemic delivery of anti-miRNA for cancer targeting and inhibition without ligand. *ACS Nano* **13**, 706–717 (2019).
98. Esposito, C. L. et al. A neutralizing RNA aptamer against EGFR causes selective apoptotic cell death. *PLoS ONE* **6**, e24071 (2011).
99. Shigdar, S. et al. RNA aptamer against a cancer stem cell marker epithelial cell adhesion molecule. *Cancer Sci.* **102**, 991–998 (2011).
100. Spencer, C. M. & Faulds, D. Paclitaxel. A review of its pharmacodynamic and pharmacokinetic properties and therapeutic potential in the treatment of cancer. *Drugs* **48**, 794–847 (1994).
101. Singh, S. & Dash, A. K. Paclitaxel in cancer treatment: perspectives and prospects of its delivery challenges. *Crit. Rev. Ther. Drug Carr. Syst.* **26**, 333–372 (2009).
102. Bailly, C. Irinotecan: 25 years of cancer treatment. *Pharmacol. Res.* **148**, 104398 (2019).
103. Schultz, A. G. Camptothecin. *Chem. Rev.* **73**, 385–405 (1973).
104. Muggia, F. M., Dimery, I. & Arbuck, S. G. Camptothecin and its analogs. An overview of their potential in cancer therapeutics. *Ann. N. Y. Acad. Sci.* **803**, 213–223 (1996).
105. Neises, B. & Steglich, W. Simple method for the esterification of carboxylic acids. *Angew. Chem. Int. Ed. Engl.* **17**, 522–524 (1978).
106. Peer, D. et al. Nanocarriers as an emerging platform for cancer therapy. *Nat. Nanotechnol.* **2**, 751–760 (2007).
107. Bangham, A. D., Standish, M. M. & Watkins, J. C. Diffusion of univalent ions across the lamellae of swollen phospholipids. *J. Mol. Biol.* **13**, 238–252 (1965).
108. Mehta, M. et al. Lipid-based nanoparticles for drug/gene delivery: an overview of the production techniques and difficulties encountered in their industrial development. *ACS Mater. Au* **3**, 600–619 (2023).
109. Yingchoncharoen, P., Kalinowski, D. S. & Richardson, D. R. Lipid-based drug delivery systems in cancer therapy: what is available and what is yet to come. *Pharmacol. Rev.* **68**, 701–787 (2016).
110. Sheoran, S., Arora, S., Samsonraj, R., Govindaiah, P. & Vuree, S. Lipid-based nanoparticles for treatment of cancer. *Heliyon* **8**, e09403 (2022).
111. Lin, X. et al. Lipid nanoparticles for chemotherapeutic applications: strategies to improve anticancer efficacy. *Expert Opin. Drug Deliv.* **9**, 767–781 (2012).
112. Haider, M., Abdin, S. M., Kamal, L. & Orive, G. Nanostructured lipid carriers for delivery of chemotherapeutics: a review. *Pharmaceutics* **12**, 288 (2020).
113. van der Koog, L., Gandek, T. B. & Nagelkerke, A. Liposomes and extracellular vesicles as drug delivery systems: a comparison of composition, pharmacokinetics, and functionalization. *Adv. Healthc. Mater.* **11**, e2100639 (2022).
114. Sercombe, L. et al. Advances and challenges of liposome assisted drug delivery. *Front. Pharmacol.* **6**, 286 (2015).
115. Inglut, C. T. et al. Immunological and toxicological considerations for the design of liposomes. *Nanomaterials* **10**, 190 (2020).
116. Alavi, M. & Hamidi, M. Passive and active targeting in cancer therapy by liposomes and lipid nanoparticles. *Drug Metab Pers Ther.* https://doi.org/10.1515/dmpt-2018-0032 (2019).
117. Garcia-Pinel, B. et al. Lipid-based nanoparticles: application and recent advances in cancer treatment. *Nanomaterials* **9**, 638 (2019).
118. Yousefi Rizi, H. A., Hoon Shin, D. & Yousefi Rizi, S. Polymeric nanoparticles in cancer chemotherapy: a narrative review. *Iran. J. Public Health* **51**, 226–239 (2022).
119. Rosenblum, D., Joshi, N., Tao, W., Karp, J.M. & Peer, D. Progress and challenges towards targeted delivery of cancer therapeutics. *Nat Commun.* **22**, 1410 (2018).
120. Beach, M. A. et al. Polymeric nanoparticles for drug delivery. *Chem. Rev.* **124**, 5505–5616 (2024).
121. Salari, N. et al. Polymer-based drug delivery systems for anticancer drugs: a systematic review. *Cancer Treat. Res. Commun.* **32**, 100605 (2022).
122. Shah, A. S., Surnar, B., Kolishetti, N. & Dhar, S. Intersection of inorganic chemistry and nanotechnology for the creation of new cancer therapies. *Acc. Mater. Res.* **3**, 283–296 (2022).
123. Khorenko, M. et al. Theranostic inorganic-organic hybrid nanoparticles with a cocktail of chemotherapeutic and cytostatic drugs. *J. Mater. Chem. B* **11**, 3635–3649 (2023).
124. Barbero, F., Gul, S., Perrone, G. & Fenoglio, I. Photoresponsive inorganic nanomaterials in oncology. *Technol. Cancer Res. Treat.* **22**, 15330338231192850 (2023).
125. Alkilany, A. M. et al. PLGA-gold nanocomposite: preparation and biomedical applications. *Pharmaceutics* **14**, 660 (2022).
126. Hoogenboezem, E. N. & Duvall, C. L. Harnessing albumin as a carrier for cancer therapies. *Adv. Drug Deliv. Rev.* **130**, 73–89 (2018).
127. Kong, L. et al. Gemcitabine-loaded albumin nanoparticle exerts an antitumor effect on gemcitabine-resistant pancreatic cancer cells induced by MDR1 and MRP1 overexpression in vitro. *Front. Surg.* **9**, 890412 (2022).
128. Kunde, S. S. & Wairkar, S. Targeted delivery of albumin nanoparticles for breast cancer: a review. *Colloids Surf. B Biointerfaces* **213**, 112422 (2022).
129. Hirsh, V. nab-paclitaxel for the management of patients with advanced non-small-cell lung cancer. *Expert Rev. Anticancer Ther.* **14**, 129–141 (2014).

130. Gradishar, W. J. Albumin-bound paclitaxel: a next-generation taxane. *Expert Opin. Pharmacother.* **7**, 1041–1053 (2006).
131. Lee, H. et al. Efficacy and safety of nanoparticle-albumin-bound paclitaxel compared with solvent-based taxanes for metastatic breast cancer: a meta-analysis. *Sci. Rep.* **10**, 530 (2020).
132. Alhebshi, S. A. et al. Toxicity of nab-paclitaxel compared to paclitaxel in a tertiary hospital in Jeddah, Saudi Arabia: a retrospective cohort study. *Cureus* **15**, e39872 (2023).
133. Dumontet, C., Reichert, J. M., Senter, P. D., Lambert, J. M. & Beck, A. Antibody-drug conjugates come of age in oncology. *Nat. Rev. Drug Discov.* **22**, 641–661 (2023).
134. Chau, C. H., Steeg, P. S. & Figg, W. D. Antibody-drug conjugates for cancer. *Lancet* **394**, 793–804 (2019).
135. Seeman, N. C. Nanomaterials based on DNA. *Annu. Rev. Biochem.* **79**, 65–87 (2010).
136. Seeman, N. C. Nucleic acid junctions and lattices. *J. Theor. Biol.* **99**, 237–247 (1982).
137. Rothemund, P. W. Folding DNA to create nanoscale shapes and patterns. *Nature* **440**, 297–302 (2006).
138. Seeman, N. & Sleiman, H. DNA nanotechnology. *Nat. Rev. Mater.* **3**, 17068 (2017).
139. Saito, S. SELEX-based DNA aptamer selection: a perspective from the advancement of separation techniques. *Anal. Sci.* **37**, 17–26 (2021).
140. Jiang, Q. et al. DNA origami as a carrier for circumvention of drug resistance. *J. Am. Chem. Soc.* **134**, 13396–13403 (2012).
141. Wang, J. et al. DNA nanobarrel-based drug delivery for paclitaxel and doxorubicin. *Chembiochem* **24**, e202300424 (2023).
142. Zhang, X. Q. et al. Strategy for increasing drug solubility and efficacy through covalent attachment to polyvalent DNA-nanoparticle conjugates. *ACS Nano* **5**, 6962–6970 (2011).
143. Hao, C. et al. Construction of RNA nanocages by re-engineering the packaging RNA of Phi29 bacteriophage. *Nat. Commun.* **5**, 3890–3897 (2014).
144. Yu, J., Liu, Z., Jiang, W., Wang, G. & Mao, C. De novo design of an RNA tile that self-assembles into a homo-octameric nanoprism. *Nat. Commun.* **6**, 5724 (2015).
145. Severcan, I. et al. A polyhedron made of tRNAs. *Nat. Chem.* **2**, 772–779 (2010).
146. Grabow, W. W. et al. Self-assembling RNA nanorings based on RNAI/II inverse cissing Complexes. *Nano Lett.* **11**, 878–887 (2011).
147. Hoiberg, H. C., Sparvath, S. M., Andersen, V. L., Kjems, J. & Andersen, E. S. An RNA origami octahedron with intrinsic siRNAs for potent gene knockdown. *Biotechnol. J.* **14**, e1700634 (2019).
148. Stewart, J. M. et al. Programmable RNA microstructures for coordinated delivery of siRNAs. *Nanoscale* **8**, 17542–17550 (2016).
149. Afonin, K. A. et al. In vitro assembly of cubic RNA-based scaffolds designed in silico. *Nat. Nanotechnol.* **5**, 676–682 (2010).
150. Bila, D., Radwan, Y., Dobrovolskaia, M. A., Panigaj, M. & Afonin, K. A. The recognition of and reactions to nucleic acid nanoparticles by human immune cells. *Molecules* **26**, 4231 (2021).
151. Hansen, A. L. & Al-Hashimi, H. M. Dynamics of large elongated RNA by NMR carbon relaxation. *J. Am. Chem. Soc.* **129**, 16072–16082 (2007).
152. Zhao, L. & Xia, T. Direct revelation of multiple conformations in RNA by femtosecond dynamics. *J. Am. Chem. Soc.* **129**, 4118–4119 (2007).
153. Hall, K. B. RNA in motion. *Curr. Opin. Chem. Biol.* **12**, 612–618 (2008).
154. Al-Hashimi, H. M. & Walter, N. G. RNA dynamics: it is about time. *Curr. Opin. Struct. Biol.* **18**, 321–329 (2008).
155. Li, H. et al. RNA as a stable polymer to build controllable and defined nanostructures for material and biomedical applications. *Nano Today* **10**, 631–655 (2015).
156. Harkness, R. W. T. & Mittermaier, A. K. G-quadruplex dynamics. *Biochim. Biophys. Acta Proteins Proteom.* **1865**, 1544–1554 (2017).
157. Danchin, A. A dynamic molecular model for transfer RNA. *FEBS Lett.* **13**, 152–156 (1971).
158. Jacobson, D. R., McIntosh, D. B., Stevens, M. J., Rubinstein, M. & Saleh, O. A. Single-stranded nucleic acid elasticity arises from internal electrostatic tension. *Proc. Natl Acad. Sci. USA* **114**, 5095–5100 (2017).
159. Hopfinger, M. C., Kirkpatrick, C. C. & Znosko, B. M. Predictions and analyses of RNA nearest neighbor parameters for modified nucleotides. *Nucleic Acids Res.* **48**, 8901–8913 (2020).
160. Adams, M. S. & Znosko, B. M. Thermodynamic characterization and nearest neighbor parameters for RNA duplexes under molecular crowding conditions. *Nucleic Acids Res.* **47**, 3658–3666 (2019).
161. Xia, T. et al. Thermodynamic parameters for an expanded nearest-neighbor model for formation of RNA duplexes with Watson-Crick base pairs. *Biochemistry* **37**, 14719–14735 (1998).
162. Dubey, A. & Bandyopadhyay, M. DNA breathing dynamics under periodic forcing: study of several distribution functions of relevant Brownian functionals. *Phys. Rev. E* **100**, 052107 (2019).
163. Cao, S. & Chen, S. J. Predicting RNA pseudoknot folding thermodynamics. *Nucleic Acids Res.* **34**, 2634–2652 (2006).
164. Staple, D. W. & Butcher, S. E. Pseudoknots: RNA structures with diverse functions. *PLoS Biol.* **3**, e213 (2005).
165. Wyatt, J. R., Puglisi, J. D. & Tinoco, I. Jr. RNA folding: pseudoknots, loops and bulges. *Bioessays* **11**, 100–106 (1989).
166. Ottink, O. M. et al. Ligand-induced folding of the guanine-sensing riboswitch is controlled by a combined predetermined induced fit mechanism. *RNA* **13**, 2202–2212 (2007).
167. Williamson, J. R. Induced fit in RNA-protein recognition. *Nat. Struct. Biol.* **7**, 834–837 (2000).
168. Ribas de Pouplana, L., Auld, D. S., Kim, S. & Schimmel, P. A mechanism for reducing entropic cost of induced fit in protein—RNA recognition. *Biochemistry* **35**, 8095–8102 (1996).
169. Haller, A., Rieder, U., Aigner, M., Blanchard, S. C. & Micura, R. Conformational capture of the SAM-II riboswitch. *Nat. Chem. Biol.* **7**, 393–400 (2011).
170. Pitici, F., Beveridge, D. L. & Baranger, A. M. Molecular dynamics simulation studies of induced fit and conformational capture in U1A-RNA binding: do molecular substates code for specificity?. *Biopolymers* **65**, 424–435 (2002).
171. Leulliot, N. & Varani, G. Current topics in RNA-protein recognition: control of specificity and biological function through induced fit and conformational capture. *Biochemistry* **40**, 7947–7956 (2001).
172. Tinoco, I. Jr., Li, P. T. & Bustamante, C. Determination of thermodynamics and kinetics of RNA reactions by force. *Q. Rev. Biophys.* **39**, 325–360 (2006).
173. Harlepp, S. et al. Probing complex RNA structures by mechanical force. *Eur. Phys. J. E Soft Matter* **12**, 605–615 (2003).
174. Higgs, P. G. & Lehman, N. The RNA world: molecular cooperation at the origins of life. *Nat. Rev. Genet.* **16**, 7–17 (2015).
175. Altman, S. The RNA-protein world. *RNA* **19**, 589–590 (2013).
176. Cech, T. R. The RNA worlds in context. *Cold Spring Harb. Perspect. Biol.* **4**, a006742 (2012).
177. Rychahou, P. et al. Colorectal cancer lung metastasis treatment with polymer-drug nanoparticles. *J. Control. Release* **275**, 85–91 (2018).
178. Tarapore, P., Shu, Y., Guo, P. & Ho, S. M. Application of Phi29 motor pRNA for targeted therapeutic delivery of siRNA silencing metallothionein-IIA and survivin in ovarian cancers. *Mol. Ther.* **19**, 386–394 (2011).
179. Pi, F. et al. RNA nanoparticles harboring annexin A2 aptamer can target ovarian cancer for tumor-specific doxorubicin delivery. *Nanomedicine* **13**, 1183–1193 (2017).
180. Guo, S. et al. Tuning the size, shape and structure of RNA nanoparticles for favorable cancer targeting and immunostimulation. *Wiley Interdiscip. Rev. Nanomed. Nanobiotechnol.* **12**, e1582 (2020).
181. Rebolledo, L. P. et al. Nucleic acid nanobiosystems for cancer theranostics: an overview of emerging trends and challenges. *Nanomedicine* **20**, 1281–1298 (2025).
182. Yip, T., Qi, X., Yan, H. & Chang, Y. Therapeutic applications of RNA nanostructures. *RSC Adv.* **14**, 28807–28821 (2024).
183. Li, X., Vieweger, M. & Guo, P. Self-assembly of four generations of RNA dendrimers for drug shielding with controllable layer-by-layer release. *Nanoscale* **12**, 16514–16525 (2020).
184. Hardonk, M. J., Harms, G. & Koudstaal, J. Zonal heterogeneity of rat hepatocytes in the in vivo uptake of 17 nm colloidal gold granules. *Histochemistry* **83**, 473–477 (1985).
185. Haseltine, W. A., Hazel, K. & Patarca, R. RNA structure: past, future, and gene therapy applications. *Int. J. Mol. Sci.* **26**, 110 (2024).
186. Biesiada, M., Pachulska-Wieczorek, K., Adamiak, R. W. & Purzycka, K. J. RNAComposer and RNA 3D structure prediction for nanotechnology. *Methods* **103**, 120–127 (2016).
187. Cheng, C. Y., Chou, F. C. & Das, R. Modeling complex RNA tertiary folds with Rosetta. *Methods Enzymol.* **553**, 35–64 (2015).
188. Wang, W. et al. trRosettaRNA: automated prediction of RNA 3D structure with transformer network. *Nat. Commun.* **14**, 7266 (2023).
189. Zhou, Y. & Chen, S. J. Harnessing computational approaches for RNA-targeted drug discovery. *RNA Nanomed.* **1**, 1–15 (2024).
190. Liu, J. et al. Fabrication of stable and RNase-resistant RNA nanoparticles active in gearing the nanomotors for viral DNA packaging. *ACS Nano* **5**, 237–246 (2011).
191. Pallan, P. S. et al. Unexpected origins of the enhanced pairing affinity of 2'-fluoro-modified RNA. *Nucleic Acids Res.* **39**, 3482–3495 (2011).
192. Xu, X., Dickey, D. D., Chen, S. J. & Giangrande, P. H. Structural computational modeling of RNA aptamers. *Methods* **103**, 175–179 (2016).
193. Boniecki, M. J. et al. SimRNA: a coarse-grained method for RNA folding simulations and 3D structure prediction. *Nucleic Acids Res.* **44**, e63 (2016).
194. Magnus, M., Boniecki, M. J., Dawson, W. & Bujnicki, J. M. SimRNAweb: a web server for RNA 3D structure modeling with optional restraints. *Nucleic Acids Res.* **44**, W315–W319 (2016).
195. Zhang, D. & Chen, S. J. IsRNA: an iterative simulated reference state approach to modeling correlated interactions in RNA folding. *J. Chem. Theory Comput.* **14**, 2230–2239 (2018).
196. Cruz, J. A. et al. *RNA-Puzzles*: a CASP-like evaluation of RNA three-dimensional structure prediction. *RNA* **18**, 610–625 (2012).
197. Sun, L. Z., Jiang, Y., Zhou, Y. & Chen, S. J. RLDOCK: a new method for predicting RNA-ligand interactions. *J. Chem. Theory Comput.* **16**, 7173–7183 (2020).
198. Zhang, S., Cheng, Y., Guo, P. & Chen, S. J. VfoldMCPX: predicting multistrand RNA complexes. *RNA* **28**, 596–608 (2022).
199. Park, H. S. et al. High EGFR gene copy number predicts poor outcome in triple-negative breast cancer. *Mod. Pathol.* **27**, 1212–1222 (2014).
200. Soria, J. C. et al. Osimertinib in untreated EGFR-mutated advanced non-small-cell lung cancer. *N. Engl. J. Med.* **378**, 113–125 (2018).
201. Rockey, W. M. et al. Rational truncation of an RNA aptamer to prostate-specific membrane antigen using computational structural modeling. *Nucleic Acid Ther.* **21**, 299–314 (2011).
202. Seifert, R., Alberts, I. L., Afshar-Oromieh, A. & Rahbar, K. Prostate cancer theranostics: PSMA targeted therapy. *PET Clin.* **16**, 391–396 (2021).
203. Wang, F., Li, Z., Feng, X., Yang, D. & Lin, M. Advances in PSMA-targeted therapy for prostate cancer. *Prostate Cancer Prostatic Dis.* **25**, 11–26 (2022).
204. Zhou, J. & Rossi, J. Aptamers as targeted therapeutics: current potential and challenges. *Nat. Rev. Drug Discov.* **16**, 181–202 (2017).

205. Yu, L., Chen, L., Satyabola, D., Prasad, A. & Yan, H. NucleoCraft: the art of stimuli-responsive precision in DNA and RNA bioengineering. *BME Front.* **5**, 0050 (2024).
206. Sabir, F. et al. DNA based and stimuli-responsive smart nanocarrier for diagnosis and treatment of cancer: applications and challenges. *Cancers* **13**, 3396 (2021).
207. Rychahou, P. et al. pH-responsive bond as a linker for the release of chemical drugs from RNA-drug complexes in endosome or lysosome. *RNA Nanomed.* **1**, 91–108 (2024).
208. Zhu, S. et al. Stimuli-responsive aptamer-drug conjugates for targeted drug delivery and controlled drug release. *Adv. Healthc. Mater.* **13**, e2401020 (2024).
209. Thomas, R. G., Surendran, S. P. & Jeong, Y. Y. Tumor microenvironment-stimuli responsive nanoparticles for anticancer therapy. *Front. Mol. Biosci.* **7**, 610533 (2020).
210. Dong, X., Brahma, R. K., Fang, C. & Yao, S. Q. Stimulus-responsive self-assembled prodrugs in cancer therapy. *Chem. Sci.* **13**, 4239–4269 (2022).
211. Rautio, J. et al. Prodrugs: design and clinical applications. *Nat. Rev. Drug Discov.* **7**, 255–270 (2008).
212. Festa, R. A. & Thiele, D. J. Copper: an essential metal in biology. *Curr. Biol.* **21**, R877–R883 (2011).
213. Cervantes-Cervantes, M. P., Calderon-Salinas, J. V., Albores, A. & Munoz-Sanchez, J. L. Copper increases the damage to DNA and proteins caused by reactive oxygen species. *Biol. Trace Elem. Res.* **103**, 229–248 (2005).
214. Binzel, D. W., Khisamutdinov, E. F. & Guo, P. Entropy-driven one-step formation of Phi29 pRNA 3WJ from three RNA fragments. *Biochemistry* **53**, 2221–2231 (2014).
215. Binzel, D. W. & Guo, P. Synergistic RNA particles for spontaneous and specific cancer targeting but low toxicity due to motility and deformation. *Nanomedicine* **20**, 1513–1515 (2025).

Acknowledgements

We thank J. Carroll for his comments on this manuscript ahead of submission. This Protocol is a comprehensive outcome supported by many years of funding from the NIH. During the preparation and revision of this manuscript, T.Y. and K.J. were supported in part by the President Research Excellence Catalyst Award to P.G. from OSU; and effort in part to P.G. and D.W.B. by R01CA293945 and R01CA257961, respectively.

Author contributions

P.G. and D.W.B. conceived and led the project. D.W.B., K.J. and Y.T. designed and conducted the experiments and co-wrote the manuscript with P.G.

Competing interests

P.G. is the licenser of Oxford Nanopore Technologies; co-founder of ExonanoRNA, LLC; and a consultant for RNA Nanobiotics.

Additional information

Supplementary information The online version contains supplementary material available at https://doi.org/10.1038/s41596-025-01306-w.

Correspondence and requests for materials should be addressed to Daniel W. Binzel or Peixuan Guo.

Peer review information *Nature Protocols* thanks Yuting Wen, Alex G. Hamilton, Xiangang Huang, Jinhwan Kim, Jong Bum Lee and the other, anonymous, reviewer(s) for their contribution to the peer review of this work.